Seismic and seafloor evidence for free gas, gas hydrates, and fluid seeps on the transform margin offshore Cape Mendocino

Anne M. Tréhu,[1] Debra S. Stakes,[2] Cindy D. Bartlett,[1,3] Johanna Chevallier,[1] Robert A. Duncan,[1] Shana K. Goffredi,[2] Susan M. Potter,[1] and Karen A. Salamy[2]

[1] Seismic data and seafloor samples indicate the presence of free gas, gas hydrate, and fluid seeps south of the Gorda Escarpment, a topographic feature that marks the eastern end of the Gorda/Pacific transform plate boundary southwest of Cape Mendocino, California. In spite of high sedimentation rates and high biological productivity, direct or indirect indicators of gas hydrate presence had not previously been recognized in this region, or along transform margins in general. Gas is indicated by a bottom simulating reflection (BSR) observed near the Gorda Escarpment, by "bright spots" and "gas curtains" scattered throughout the sedimentary basin to the south, and by $\delta^{13}C$ and $\delta^{18}O$ isotopes of carbonates, which are similar to those recovered from other hydrate-bearing regions. The BSR reflection coefficient of -0.13 ± 0.04 and interval velocities as low as 1.38 km/s indicate that free gas is present beneath the BSR. Local shallowing of the BSR toward the north facing Gorda Escarpment and beneath a channel near the crest suggests fluid flow toward the seafloor. Integrating these various observations, we suggest a scenario in which methane is formed in thick Miocene and Pliocene deposits of organic-rich sediments that fill the marginal basin south of the transform fault. Dissolved and free gas migrates toward the escarpment along stratigraphic horizons, resulting in hydrate formation and in channels, slumps and chemosynthetic communities on the face of the escarpment. We conclude that the BSR appears where hydrate-bearing sediments are uplifted because of current triple junction tectonics.   *INDEX TERMS:* 0930 Exploration Geophysics: Oceanic structures; 1040 Geochemistry: Isotopic composition/chemistry; 3025 Marine Geology and Geophysics: Marine seismics (0935); 3045 Marine Geology and Geophysics: Seafloor morphology and bottom photography; 8150 Tectonophysics: Plate boundary—general (3040); *KEYWORDS:* Mendocino transform fault, gas hydrates, seismic imaging

1. Introduction

[2] The Mendocino transform fault is the boundary between the Pacific plate to the south and the Gorda/Juan de Fuca plate to the north. East of 126°W, the Pacific plate is shallower than predicted based on its age, rising up to 1 km above the younger Gorda plate to the north [*Leitner et al.*, 1998] and forming a structural feature known as the Gorda Escarpment. In May 1999, we conducted a seismic reflection survey of the Gorda Escarpment to map stratigraphy and structure on the southern flank of the escarpment and tie the seismic stratigraphy to results of drilling at ODP site 1022 (Figure 1). Approximately 1500 km of seismic reflection data were acquired using a six-gun, 22.1-L tuned air gun array source and a 480-channel, 6-km-long streamer. New swath bathymetric data were also acquired.

[3] We were surprised to see a bottom simulating reflection (BSR) near the eastern end of the escarpment because BSRs have not previously been reported from transform plate boundaries (see the recent global compilation of *Kvenvolden and Lorenson* [2001], who cite examples of BSRs from accretionary complexes, passive margins, marginal basins, and inland seas). BSRs attributable to gas hydrates are negative-polarity seismic reflections that cut across stratigraphic horizons and are approximately parallel to the seafloor at the depth at which gas hydrate is predicted to no longer be stable because of increasing temperature with depth beneath the seafloor [e.g., *Shipley et al.*, 1979]. The negative polarity of the BSR indicates that the reflection results from a decrease in seismic velocity and/or density at this depth. Many studies have concluded that the reflection results from the combined effect of hydrate within the stability zone, which increases seismic velocity, and free gas below the stability zone, which decreases

---

[1] College of Oceanic and Atmospheric Sciences, Oregon State University, Corvallis, Oregon, USA.

[2] Monterey Bay Aquarium Research Institute, Moss Landing, California, USA.

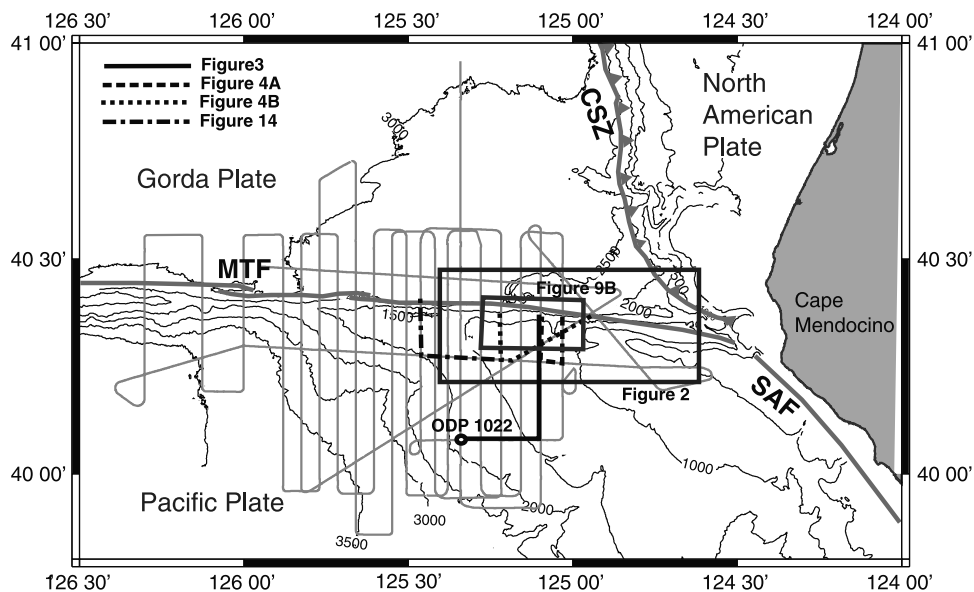[3] Now at AMEC, Portland, Oregon, USA.

Figure 1. Topographic map of the Mendocino triple junction region. Plate boundaries are shown as thick gray lines. Light gray lines represent seismic profiles acquired during cruise EW9905. The large box outlines the region shown in Figure 2a; the small box corresponds to Figure 9b. The locations of ODP site 1022 and of the seismic profiles shown in Figures 3, 4, and 14 are also shown. MTF, Mendocino transform fault; CSZ, deformation front of the Cascadia subduction zone; SAF, San Andreas Fault.

seismic velocity [e.g., *Bangs et al.*, 1993; *Singh et al.*, 1993; *Tréhu et al.*, 1995; *Holbrook et al.*, 1996; *Korenaga et al.*, 1997; *Yuan et al.*, 1999; *Pecher et al.*, 2001; *Holbrook*, 2001].

[4] Estimation of the global inventory of methane stored in gas hydrates and as free gas below the hydrate stability zone is important for testing models of the impact of gas hydrates on global climate change [e.g., *Revelle*, 1983; *Dickens*, 2001]. The presence of a BSR remains the primary proxy for gas hydrate presence in the absence of direct observations in spite of large uncertainties in determining hydrate and gas concentration from seismic data. These uncertainties result from uncertainties about the velocity structure of comparable sediments in the absence of hydrate and free gas [*Yuan et al.*, 1996], from pressure dependence and nonlinear sensitivity of seismic parameters to gas and hydrate concentrations [e.g., *Carcione and Tinivella*, 2000; *Han and Batzle*, 2002], from uncertainties in estimating in situ concentrations in those few places where seismic estimates can be ground-truthed by direct sampling [e.g., *Paull and Ussler*, 2001], and from the fact that gas hydrate has been found in cores obtained from sites where no BSR is observed [e.g., *Kvenvolden and Kastner*, 1990; *Paull et al.*, 1996].

[5] Because of the absence of reports of BSRs from transform margins, they have not been included in global estimates of the amount of methane stored in submarine gas hydrate/free gas systems. *Lyle et al.* [2000] speculated that the apparent absence of a BSR south of the Mendocino transform fault in site survey data for ODP Leg 167, in contrast to the Cascadia subduction zone north of the transform where gas hydrates are common [e.g., *Brooks et al.*, 1991; *MacKay et al.*, 1994; *Carson et al.*, 1995; *Yuan et al.*, 1996, 1999; *Tréhu et al.*, 1999; *Suess et al.*, 2001], was due to less compression, leading to less compaction of sediments and less concentration of methane near the surface.

[6] The objective of this paper is to present new seismic evidence for the presence of free gas and gas hydrate on the northern California continental margin south of the Mendocino transform fault. It complements *Stakes et al.* [2002], who presented geologic and biologic observations of an active seep on the Gorda Escarpment. New biologic and geochemical evidence are also presented here. Integration of seismic, stratigraphic, tectonic, biological, and geochemical evidence suggests a geologic model for hydrate formation and dissociation in this tectonic setting.

2. Seafloor Morphology

[7] The morphology of the eastern end of the Gorda Escarpment is shown in Figure 2a. Near 125°W, the trend of the escarpment changes from nearly east-west to south-

Figure 2. (opposite) (a) Bathymetric map of the region where seismic indicators of gas hydrates are observed based on Hydrosweep data collected during cruise EW9905 supplemented by additional data from NOAA EEZ surveys. Light black lines show track lines for seismic and Hydrosweep data. Heavy black lines are portions of seismic lines shown in Figure 2c. The red box shows the location of Figure 9b. (b) The 3-D perspective of the region shown in Figure 2a. (c) Seismic sections across the eastern part of the Gorda Escarpment. The bottom-simulating reflection (BSR) and bright spots indicative of free gas are labeled. B1 and B2 are prominent basement features uplifted to form the escarpment and discussed in the text.
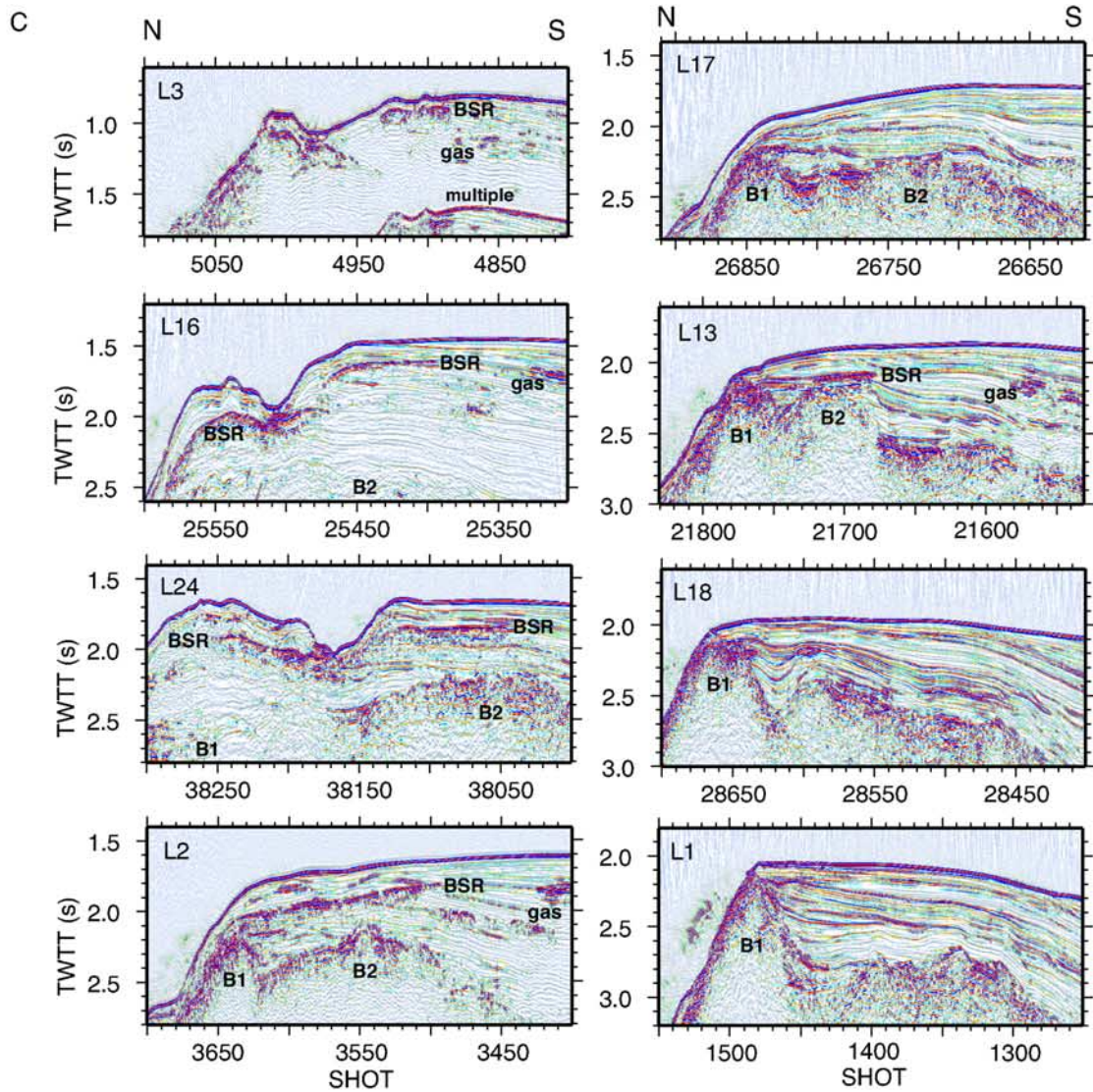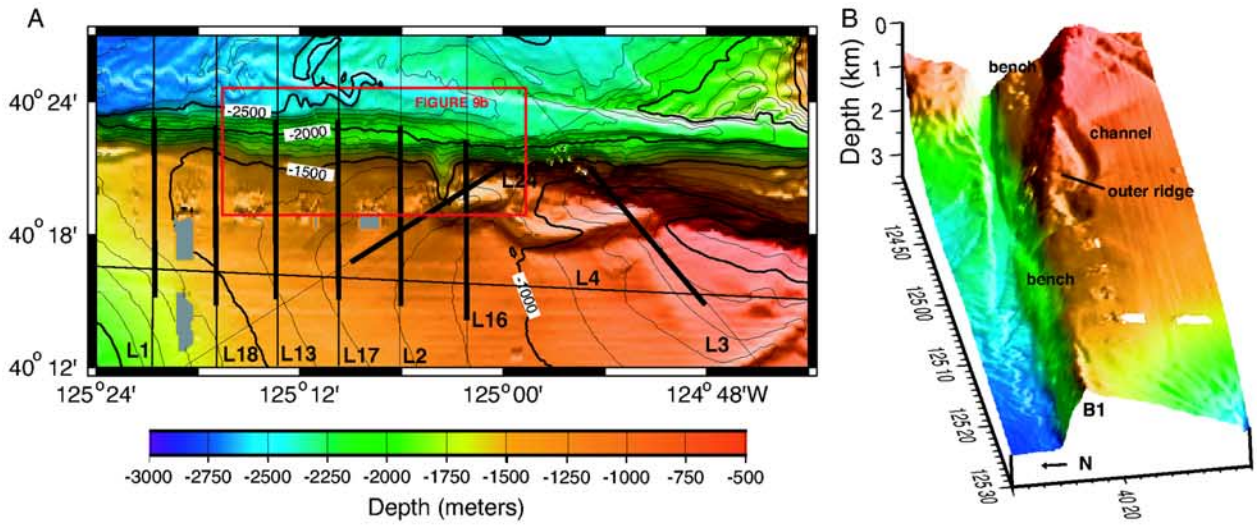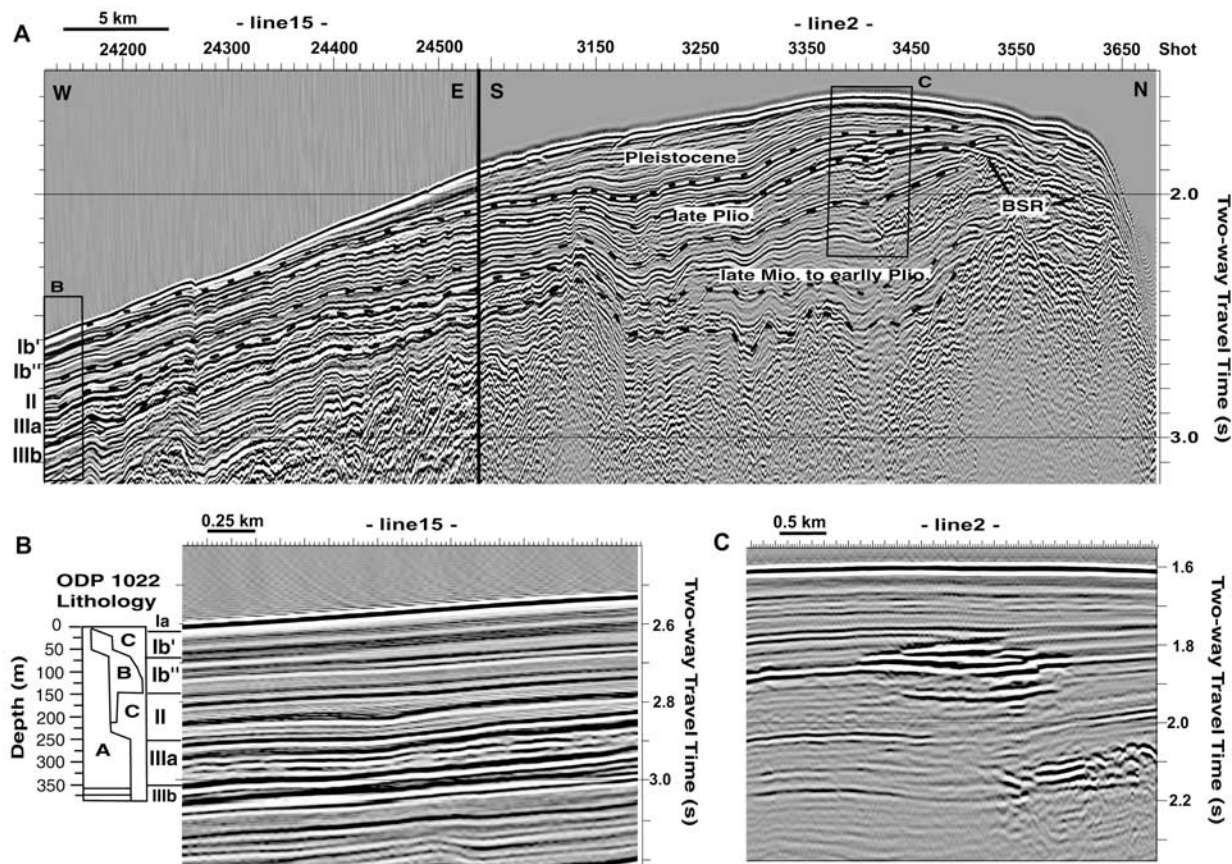
Figure 3. (a) Summary of results from ODP Site 1022 [from *Leg 167 Shipboard Scientific Party*, 1997b] compared to seismic data along lines 15 and 2. Major stratigraphic boundaries can be traced from Site 1022 to the escarpment. The position of the Plio/Pleistocene boundary is assumed based on the observation that it is effectively at the seafloor at ODP Site 1022. (b) Detail near ODP Site 1022. In the lithologic summary, A is diatom ooze, B is nannofossil ooze, and C is clay. Below 350 m, chert and porcellanite were recovered. (c) Detail of bright spot.

east. East of 125°15'W the face of the escarpment is draped by sediment, in contrast to farther west, where igneous basement is exposed along its face. An oblique lineation at the base of the escarpment suggests tectonic complexity associated with the transition from the San Andreas transform fault to the Mendocino transform fault. Topographic benches on the face of the escarpment in this region are suggestive of major mass wasting events. One of the most striking features of the eastern end of the Gorda Escarpment is a 15 km long, 2 km wide, and 100 m deep channel along its crest. This channel curves to intersect the escarpment at both ends, forming a ridge we call the "outer ridge" (Figure 2a). A possible origin for this channel, which appears similar to one recently reported by *Driscoll et al.* [2000] offshore North Carolina, is discussed in section 4. Smaller (2 km long and 200 m wide) north-south trending gullies on the face of the escarpment, which are not visible at the scale of Figure 2a, are also discussed in section 4.

3. BSRs and Bright Spots

[8] A strong BSR is seen on all but one (L17) of the seismic sections from east of 125°15'W (Figure 2b). It is observed near the escarpment and extends 3–5 km to the south. The depth of this event beneath the seafloor increases as seafloor depth increases and is generally consistent with the predicted depth to the base of the gas hydrate stability zone assuming the temperature gradient measured at ODP site 1022 (with some exceptions discussed later). Farther south, the BSR is absent but the data contain many bright spots and gas curtains characteristic of the presence of pockets of free gas in the sediments [*Hovland et al.*, 1994]. West of 125°15'W there is no negative-polarity BSR in the seismic records (L18, L1).

3.1. Stratigraphic Setting

[9] The stratigraphic setting of the sediments hosting the BSR can be determined by correlation with ODP Site 1022 (Figure 3). This site was drilled during Leg 167, the objective of which was to study the Neogene history of the California current [*Leg 167 Shipboard Scientific Party*, 1997a]. The lithologic summary for Site 1022 is shown in Figure 3b, converted into two-way travel time using a smoothed interval velocity function obtained by averaging interval velocities for several common midpoint gathers
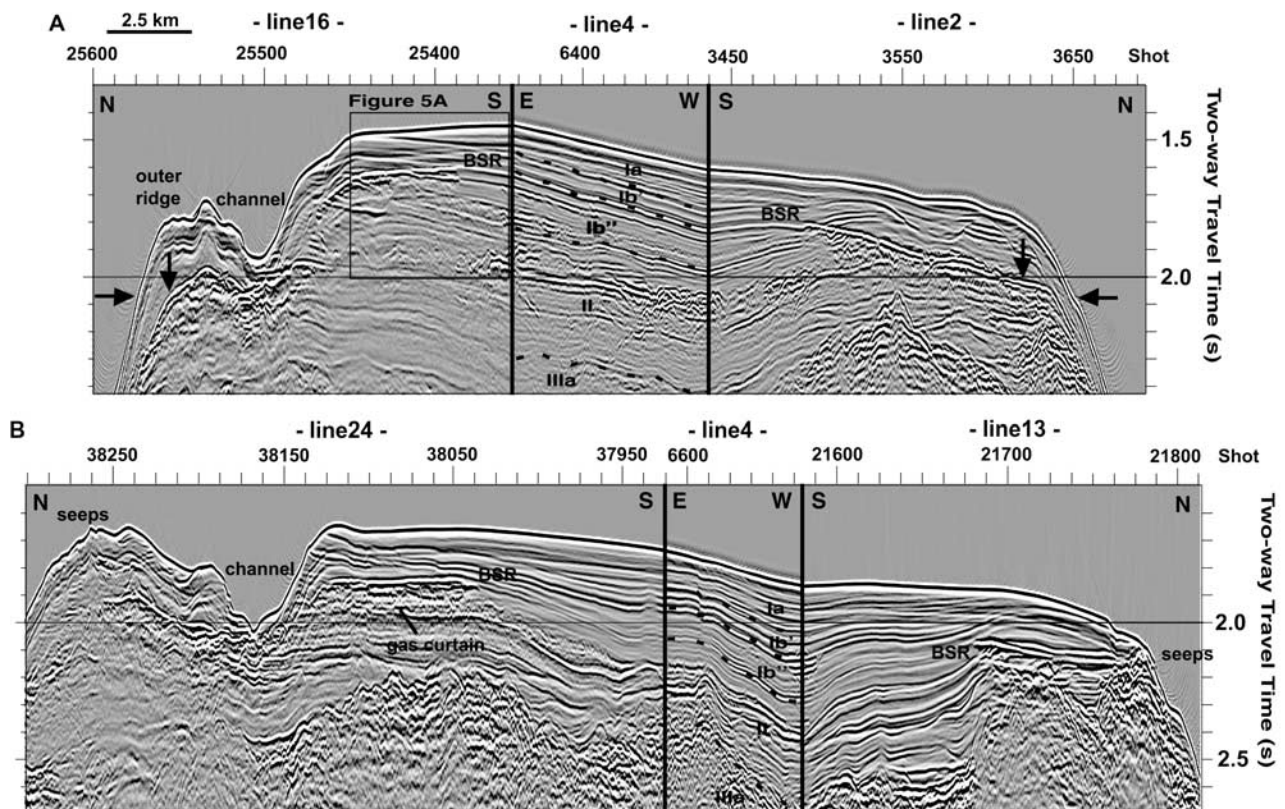
Figure 4. Seismic sections across the Gorda Escarpment that image a BSR. The stratigraphic setting, based on the correlation with ODP Site 1022 as shown in Figure 3, is indicated on line 4, which ties all profiles together. A more detailed view of the northern ends of seismic lines 16 and 24 is shown in Figure 11. Vertical arrows on lines 2 and 16 show were the BSR starts to shallow, and horizontal arrows mark the upper limit of gullies on the face of the escarpment (see section 4 of text).

(CMPs) on lines 1 (N-S) and 15 (E-W), which cross at Site 1022 (Figure 1). Maximum depth sampled in the ODP core is 388 m below the seafloor. Only a few meters of Pleistocene sediment were recovered (Unit Ia in Figure 3b, adopting the nomenclature of *Leg 167 Shipboard Scientific Party* [1997b]). Underlying this is a thick late Pliocene section characterized by a significant nannofossil component that increases down hole (Unit Ib [*Leg 167 Shipboard Scientific Party*, 1997b]). We further subdivide Unit Ib into Ib′ and Ib″ based on a significant change in clay content at ∼50 m below seafloor (mbsf) that corresponds to a regional seismic reflection. Unit II is early Pliocene clay and diatom clay with infrequent interbeds of nannofossil ooze (II in Figure 3b). The biosilicious component of the sediment increases in the early Pliocene to late Miocene sediment of Unit IIIa. Below 360 mbsf, diatomite is transformed to siliceous mudstone and chert (IIIb in Figure 3b). Dolostone layers up to a few 10s of centimeters thick occur infrequently throughout the section, with concentrations near 200 mbsf and 350 mbsf. Oxygen and carbon isotopes of these dolomites indicate that they were formed in the subsurface in a zone of methanogensis [*Stakes et al.*, 2002], consistent with high methane values measured in the cores for depths greater than 50 m [*Leg 167 Shipboard Scientific Party*, 1997b].

[10] In spite of uncertainties in the velocity, the two-way travel time (TWTT) to lithologic boundaries can be estimated to within ∼0.02 s. We have traced reflections associated with the lithological boundaries from Site 1022 along 50 km of seismic section to the Gorda Escarpment (Figures 3a and 4). Although the amplitude of some of the reflections changes along the profiles, particularly across an apparently active growth fault on line 15, most of the events can be traced unambiguously. The data indicate formation of a sedimentary basin south of the escarpment during the Pliocene. Deformation of the southern and northern boundaries of this basin was contemporaneous with deposition and is continuing along the Gorda Escarpment. The BSR is observed in uplifted Pliocene sediments of Units Ib″ and II.

[11] While it is difficult to determine the polarity of individual stratigraphic reflections, several particularly bright events appear to have negative polarity (white flanked by black for the wavelet shape and amplitude scale of these data), suggesting that they are low-velocity zones. In particular, the reflection that corresponds to the boundary between Units Ib′ and Ib″ is consistently very strong except in the immediate vicinity of Site 1022. Several bright spots (see section 3.2) are associated with this reflection. A similar regional bright reflection is observed within unit II. Such bright spots are generally attributed to pockets of

gas or aqueous fluids. We speculate that the decrease in clay content across the boundary between Unit Ib′ and Ib″ leads to permeability anisotropy that channels fluids along stratigraphic horizons basin-wide.

[12] Additional insight into the stratigraphic factors that may control fluid flow within the basin can be obtained by looking at the onshore Monterey Formation exposed near Santa Cruz, CA, which is similar in age and composition to the sediments sampled at Site 1022. The Monterey Formation contains evidence for a complicated system of fluid flow along chert-rich stratigraphic horizons and in carbonate "pipes" oriented perpendicular to strata [*Aiello et al.*, 2001]. Strontium isotopes in carbonates deposited along faults in this formation have been interpreted to indicate strong flow anisotropy, with formation-parallel flow over distances of at least 4 km and possibly >12 km, compared to distances of 700 m across strata [*Eichhubl and Boles*, 2000].

3.2. Characteristics of the Bright Spots

[13] Figure 3c shows a detail of a bright spot on line 2. This bright spot is characterized by high amplitudes, a decrease in the dominant frequency of the waveform, and apparent "velocity pull-down" and attenuation of amplitudes of horizons beneath the bright spot. All of these characteristics suggest the presence of free gas in the sediments. Assuming that the velocity of gassy sediment is 1.2 km/s and that the velocity of the adjacent sediment is 1.8 km/s, the observed pull down of 0.02–0.03 s TWTT indicates a thickness of the gas-rich zone of 160–270 m. The generally high amplitude and negative polarity of the reflection corresponding to the boundary between units 1b′ and 1b″ suggests a permeable horizon along which gas-charged fluids are migrating toward the bright spot. Another bright spot associated with this horizon is located at the intersection of lines 4 and 13 (Figure 4). In addition to the bright spots, zones of high-amplitude, scattered seismic energy, called gas curtains by *Hovland et al.* [1994], are also observed (Figures 3 and 4). Gas curtains suggest some vertical migration of gas. We note, however, that no gas or hydrate "chimneys," such as are seen in the Bering Sea [*Scholl and Hart*, 1993], on the Vancouver accretionary margin [*Riedel et al.*, 2001], on the Blake Ridge [*Gorman et al.*, 2002] and elsewhere, are observed in this region, suggesting that fluid flow and gas migration occur primarily along stratigraphic boundaries.

3.3. Characteristics of the BSR

[14] On most of the seismic lines, stratigraphic reflections approach the BSR at a low angle making it difficult to trace individual reflections across the BSR. In several cases, amplitudes of seismic reflections increase as they approach the BSR from below (e.g., horizon B in Figure 5a). Similar observations have been made elsewhere. During ODP Leg 164 to the Blake Ridge, it was determined that this amplitude pattern was due to the enhancement of reflectivity beneath the BSR by the presence of free gas [*Holbrook et al.*, 1996; *Holbrook*, 2001]. The polarity of the stratigraphic reflection that is coincident with the onset of the BSR appears to change from positive to negative (horizon A in Figure 5a),

suggesting the sudden onset of a free gas phase. This is also observed for horizon B.

3.3.1. Reflection Coefficients

[15] To compare the characteristics of the BSR on the Gorda Escarpment with observations elsewhere, we have calculated the reflection coefficient at this boundary for the portion of line 16 shown in Figure 5a. Following *Claerbout* [1976], the BSR reflection coefficient (R_{BSR}) can be calculated from the BSR amplitude and the seafloor reflection coefficient (R_{SF}): $R_{BSR} = (R_{SF}/(1 - R_{SF}^2))*(A_{BSR}/A_{SF})$, where A_{BSR} and A_{SF} are the amplitude of the BSR and seafloor, after multiplying observed amplitudes by travel time to correct for the geometrical spreading of a point source. The seafloor reflection coefficient was determined from the ratio of the corrected amplitude of the first seafloor multiple to the amplitude of the primary seafloor reflection. To empirically verify this spreading factor, we also calculated R_{SF} using the first and second multiples of the seafloor reflection. Both estimates yielded essentially the same result. R_{SF} and R_{BSR} are shown in Figure 6.

[16] The seafloor reflection coefficient of 0.27 ± 0.03 near the Gorda Escarpment is higher than "typical" seafloor reflection coefficients, which are generally 0.1–0.2 [e.g., *Katzman et al.*, 1994; *Yuan et al.*, 1999], but is similar to values obtained along the crest of accretionary ridges of the Cascadia subduction zone, where local carbonate crusts lead to reflection coefficients that are typically ~0.3 [e.g., *Fink and Spence*, 1999]. We attribute the high seafloor reflectivity south of the Gorda Escarpment primarily to the erosional nature of the seafloor, although diagenesis related to fluid flow may also be a factor. Visual observation and gravity coring of the seafloor near the crest of the escarpment during ROV dives conducted in 2000 and 2001 confirm that the seafloor is swept by currents and that Pliocene age sediments are exposed on the seafloor. Assuming a sediment density of 1500 kg/m³ and water velocity and density of 1480 m/s and 1000 kg/m³, respectively, the velocity of sediments at the seafloor required to give the observed range of reflection coefficients is 1.61–1.83 km/s.

[17] The BSR reflection coefficient of −0.13 ± 0.04 is approximately twice as large as the reflection coefficient of horizon A immediately south of the BSR onset. It is comparable to that determined for strong BSRs in accretionary complexes [e.g., *Tréhu et al.*, 1995; *Yuan et al.*, 1999; *Fink and Spence*, 1999], and slightly larger than the reflection coefficient of 0.09 ± 0.04 determined for a relatively strong BSR on the Blake Ridge [*Katzman et al.*, 1994]. Some of the lateral variability in seafloor and BSR reflection coefficients probably results from natural variations and some (for example, the low apparent seafloor reflectivity between CMP 4440 and 4510, which is closely correlated with the apparent BSR reflectivity) is probably due to interference between the seafloor reflection and reflections from underlying strata. Assuming a sub-BSR velocity of 1.4 km/s and no density contrast, this reflection coefficient implies a velocity of 1.72–1.85 km/s above the BSR.

3.3.2. Interval Velocities

[18] To test whether velocity estimates derived from reflection coefficients are reasonable and to obtain additional insight into the distribution of gas and hydrate in the
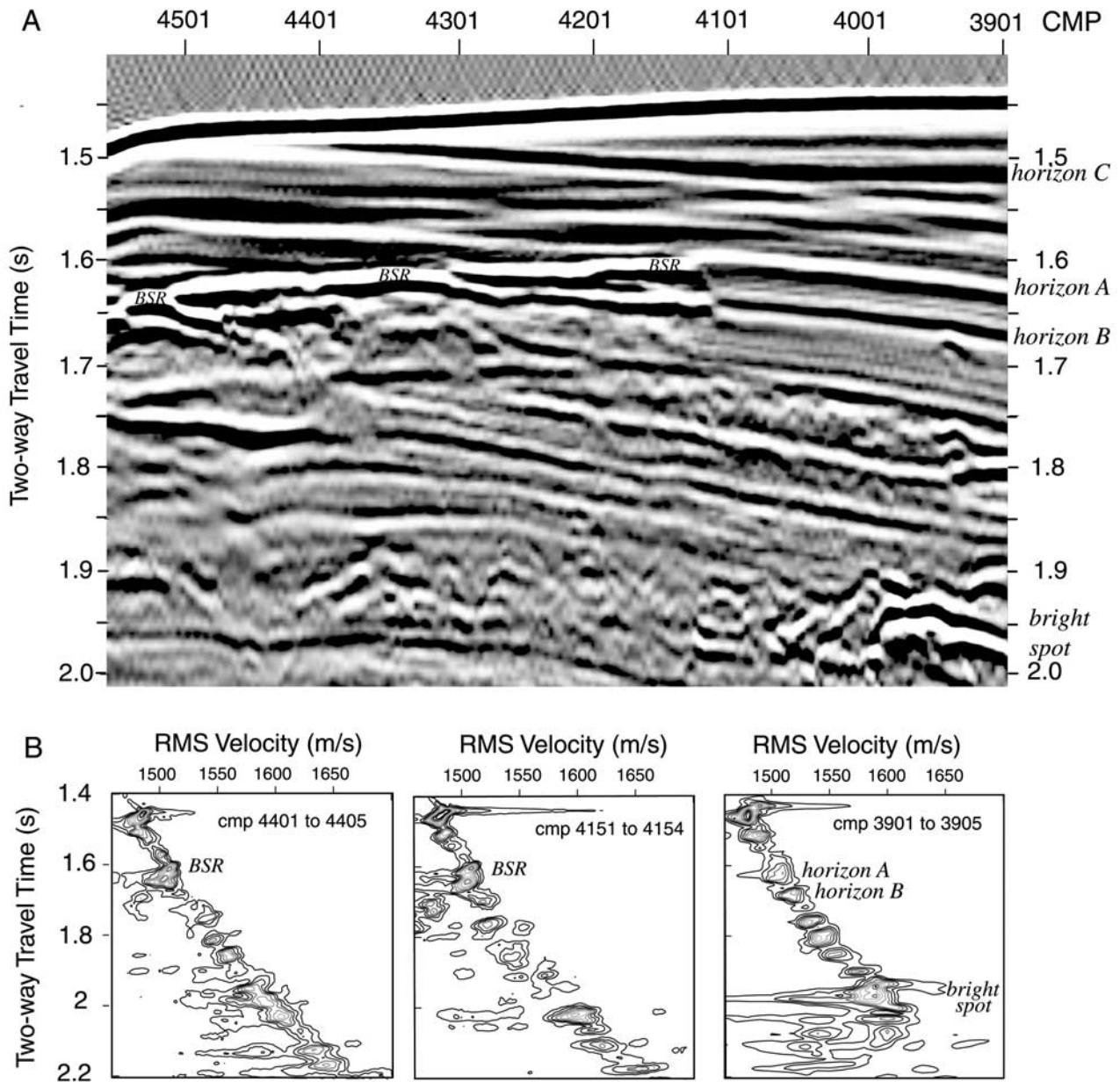
Figure 5. (a) Detail of the southern edge of the BSR on line 16. Negative polarities are white and positive polarities are black. The wavelet, as shown by the seafloor reflection, is a positive pulse flanked by two negative side lobes. Horizon A appears to be a regional negative polarity event that corresponds to the boundary between 1b′ and 1b″ at ODP Site 1022. Horizon B appears to change polarity from positive to negative as it approaches the BSR from below. Intersection of this event with the BSR results in locally low BSR amplitude. (b) Examples of typical semblance analyses. Four adjacent CMPs were used for each analysis for which velocity and time were incremented by 2 m/s and 0.02 s, respectively.

sediments, we calculated interval velocities for every 25th CMP on line 16 between CMP 3901 and 4601. Examples of semblance analyses from which stacking velocities were picked are shown in Figure 5b. CMP 3901 is from south of the BSR onset but includes a deeper bright spot. CMPs 4151 and 4401 include the BSR, and both show a second semblance peak ∼0.03 s beneath the BSR. The decrease in stacking velocity results in a very low interval velocity estimate of 1.38 km/s. This is typical of the semblance analyses where the BSR is underlain by a strong reflection (CMP 4110–430; 4400–4525). Where this subBSR reflection is not present, the interval velocity beneath the BSR is calculated over a larger interval and shows a smaller, but still distinct, decrease. In contrast, interval velocities from CMPs south of the BSR (e.g., CMP 3901 in Figure 5b) show no significant velocity inversions, except for beneath the bright spot, which indicates a velocity of ∼1.45 km/s. The interval velocity immediately above the BSR is 1.69– 1.81 km/s, consistent with the estimate derived from the reflection coefficient.
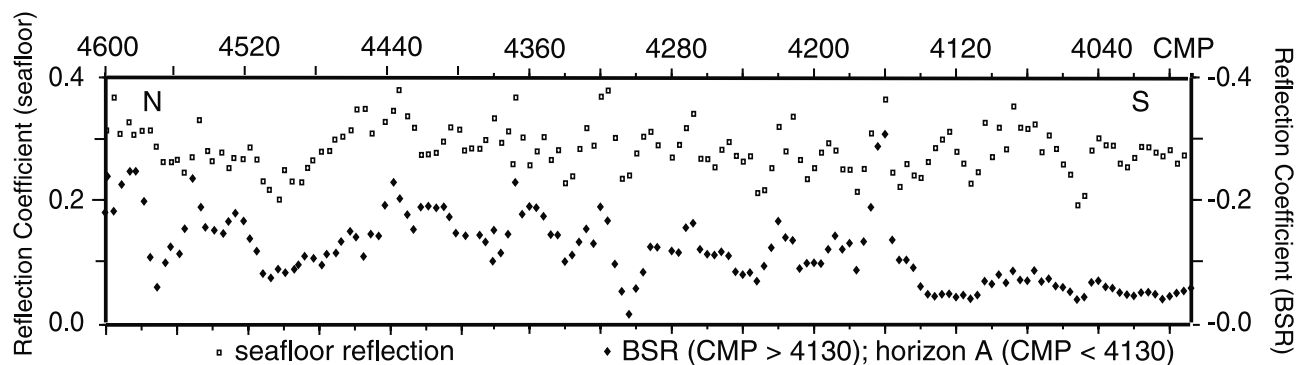
Figure 6. Reflection coefficients at the seafloor and BSR for the data shown in Figure 5a derived as discussed in the text.

[19] It is difficult to estimate the concentration of gas in the pore space from seismic observations because the seismic *P* wave velocity drops very abruptly as the percentage of free gas in the pore space increases from 0 to ~5% and increasing gas concentration has only a small effect [e.g., *Ostrander*, 1984; *Bangs et al.*, 1993; *Carcione and Tinivella*, 2000]. The velocity change from 1.8 km/s where there is no BSR to <1.4 km/s where the BSR is strong implies at least 5% free gas in the pore space distributed over up to 200–300 m beneath the BSR and the bright spot. The in situ concentration may be considerably greater. *Han and Batzle* [2002] have recently pointed out that the effect of free gas decreases as pressure increases and the gas is compressed. As more laboratory measurements of this effect become available, we may be able to more precisely estimate in situ gas concentration from seismic velocity measurements.

[20] Interval velocities in the sediments within the hydrate stability zone have been used to estimate hydrate concentrations [e.g., *Fink*, 1995; *Yuan et al.*, 1996; *Korenaga et al.*, 1997; *Spence and Fink*, 1999; *Gorman et al.*, 2002]. Here, interval velocities increase by 0.05 km/s between CMPs 4126 and 4351 compared to velocities to the south where the BSR is not present. If this increase is due to increasing hydrate concentration, an increase of ~5% is implied (following *Fink* [1995] and assuming the porosity/density relationship of *Hyndman et al.* [1993]). However, we note that the interval velocity appears to decrease by 0.05 km/s north of CMP 4351 even though the BSR is still present. This may be due to our inability to accurately pick a stacking velocity for horizon C where this reflection interferes with the seafloor reflection. It is likely that interval velocities are not precise enough to resolve small lateral variations in hydrate concentration above the hydrate stability zone here.

[21] Additional constraints on hydrate and gas distribution and concentration in this system might be obtained from detailed modeling of seismic waveforms [e.g., *Singh et al.*, 1993; *Pecher et al.*, 1996; *Korenaga et al.*, 1997; *Holbrook*, 2001] but would not significantly affect the conclusions presented here. The data generally show a large increase in BSR amplitude for incident angles greater than ~40°, supporting the conclusion that the BSR is due primarily to the presence of gas and limiting the hydrate concentration to <40% because a decrease in amplitude with offset is predicted at such high hydrate concentrations [*Carcione and Tinivella*, 2000].

3.4. Is Hydrate Required?

[22] Because some of the seismic waveform modeling studies cited in the previous section have demonstrated that the BSR waveform can, in some cases, be adequately modeled by including only the effect of free gas without requiring a velocity anomaly attributable to hydrate, some investigators have questioned the validity of the BSR as a proxy for hydrate occurrence. However, if free gas is present within a sedimentary horizon immediately beneath the seismic BSR and if the reflective pattern characteristic of free gas abruptly disappears at the predicted depth of the gas hydrate stability field, we consider that it likely that hydrate is present above the BSR. We therefore consider that the presence of a BSR is a robust proxy for the presence of hydrate within the hydrate stability zone, although absence of a BSR does not imply absence of hydrate.

[23] If the BSR develops in response to uplift (as proposed by *Pecher et al.* [1996] for the Peru margin; see also section 6 of this paper), it is possible that hydrate is present regionally within the hydrate stability zone even though the concentration may be too small to produce a seismic reflection in the absence of free gas. Modeling of hydrate formation has shown that free gas is not required for the formation of hydrate in seafloor sediments [*Rempel and Buffett*, 1997; *Zatsepina and Buffett*, 1997; *Xu and Ruppel*, 1999]. When fluids with a high concentration of dissolved methane are advected into the hydrate stability zone, a decrease in methane solubility can result in hydrate formation without the presence of free gas. In the data reported here, we note the presence of discontinuous subhorizontal reflective "lenses" between horizons A and C, which are present above, but not below, the BSR. We speculate that this reflective pattern indicates the presence of lenses of hydrate within the sediments that results from advection of methane-rich fluids in Units Ib″ and II toward the escarpment. Testing this speculation and quantifying hydrate concentration is complicated by the fact that the tectonic setting makes it difficult to find a "reference site" for determining the velocity of uplifted, hydrate-free sediments of the same age and depth of burial.

4. Fluid Flow Inferred From Variations in BSR Depth and Seafloor Morphology

[24] The depth to the base of the gas hydrate stability field depends on pressure, temperature, and gas solubility. These
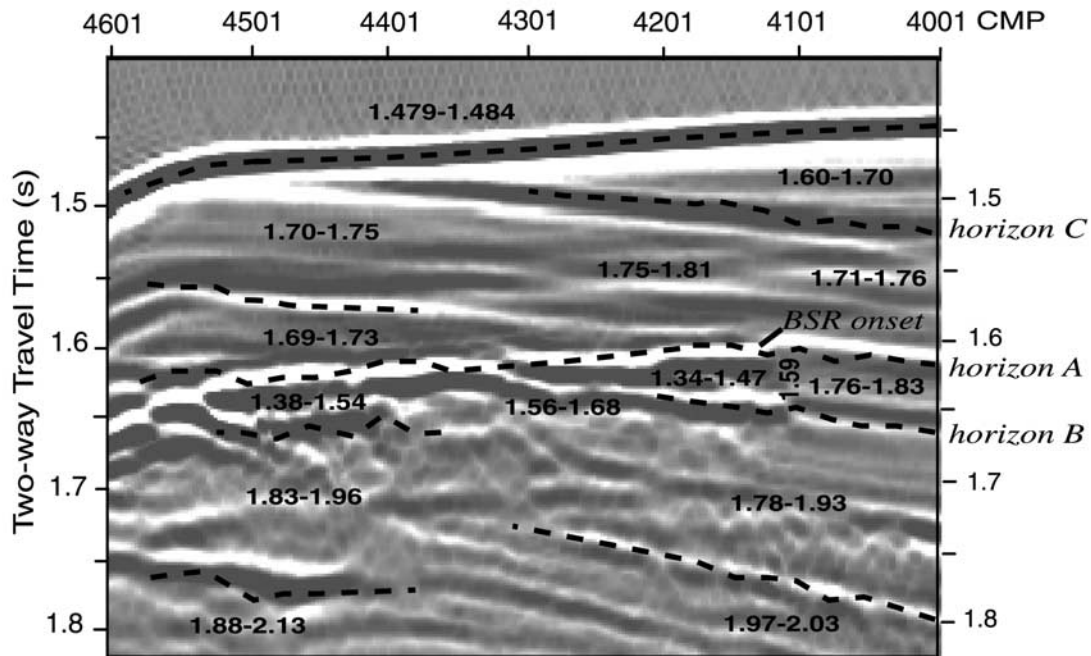
Figure 7. Summary of interval velocities obtained from stacking velocity picks at 25 CMP intervals overlain on the data shown in Figure 5a.

parameters, in turn, depend on many factors, including water depth, sediment density, seafloor temperature, geothermal gradient, pore fluid salinity, gas composition, and sediment composition and grain size [e.g., *Ruppel*, 1997; *Clennell et al.*, 1999]. In spite of uncertainties and natural variability in these parameters, apparent thermal gradients calculated from BSR depths can provide insights into subsurface temperature structure and indirectly into patterns of fluid flow [e.g., *Yamano et al.*, 1982; *Bangs et al.*, 1993; *Yuan et al.*, 1996; *Pecher et al.*, 1996; *Zwart et al.*, 1996]. We calculated the apparent thermal gradient assuming hydrostatic pressure, a sediment *P* wave velocity of 1.73 km/s (measured by interval velocity analysis; Figure 7), a seafloor temperature of 2.5°C (as was measured near the escarpment during ROV dives; Figure 8), and the phase boundary for pure methane hydrate in water of 3.5% salinity (as determined experimentally by *Maekawa et al.* [1995]).

[25] The apparent thermal gradient at the southern onset of the BSR is very similar to the thermal gradient of 0.088°/m measured at ODP site 1022 [*Leg 167 Shipboard Scientific Party*, 1997b] on all profiles (Figure 8). On L13, the apparent thermal gradient remains approximately constant to the north as the BSR disappears south of basement ridge B1. On L2, it decreases slightly toward the Gorda Escarpment and then increases as the seafloor deepens along the face of the escarpment (marked by an arrow on Figure 8). On L16, it increases to >0.150°/m beneath the topographic channel near the edge of the escarpment. This high inferred thermal gradient is similar to that calculated by *Zwart et al.* [1996] across faults on the Cascadia margin. North of the channel beneath the outer ridge (Figure 2a), the inferred thermal gradient decreases as the escarpment is approached and then increases as seafloor depth increases, similar to L2. L24 shows a similar pattern to L16 except that the BSR has a gap beneath the crest of the outer ridge.

[26] Because the sediments hosting the BSR are relatively undeformed and are almost parallel to the BSR, lateral changes in sediment properties are an unlikely explanation for the systematic lateral changes in apparent thermal gradient. Lateral changes in bottom water temperature can also be ruled out. During an ROV dive to the channel and outer ridge (Figure 9), bottom water temperature increased from 2.2° at 1700 m to 2.8° at 1350 m. If the water depth and depth to the BSR are fixed, a bottom water temperature decrease of 0.6°C results in an increase in apparent temperature gradient of 0.04°C/m. Lateral variations in water bottom temperature are therefore not adequate to explain the large increases in apparent temperature gradient beneath the channel and the face of the escarpment, which occur over a depth range of ∼100 m and bottom water temperature change of <0.3°C. Bottom water temperature changes also cannot explain the small, gradual decrease in apparent temperature gradient toward the crest of the escarpment because the observations show the opposite trend from that predicted. We conclude that the apparent temperature gradient variations in Figure 10 represent lateral changes in subsurface temperature gradient.

4.1. Diffuse Fluid Flow Toward the Escarpment

[27] The abrupt increase in the apparent thermal gradient beneath the face of the escarpment on lines 2 and 16 is interpreted to indicate diffuse flow of warm fluids from beneath the BSR to the seafloor. This interpretation is supported by the presence of erosional or drainage gullies on the face of the escarpment that are imaged in high-resolution bathymetric (Simrad EM300) data collected by MBARI in 1998 (Figure 9). These structures are observed east of 125°15'W and are not present west of 125°15'W [*Stakes et al.*, 2002]. The gullies begin at a water depth of 1600–1700 m. The spatial correlation between initiation of
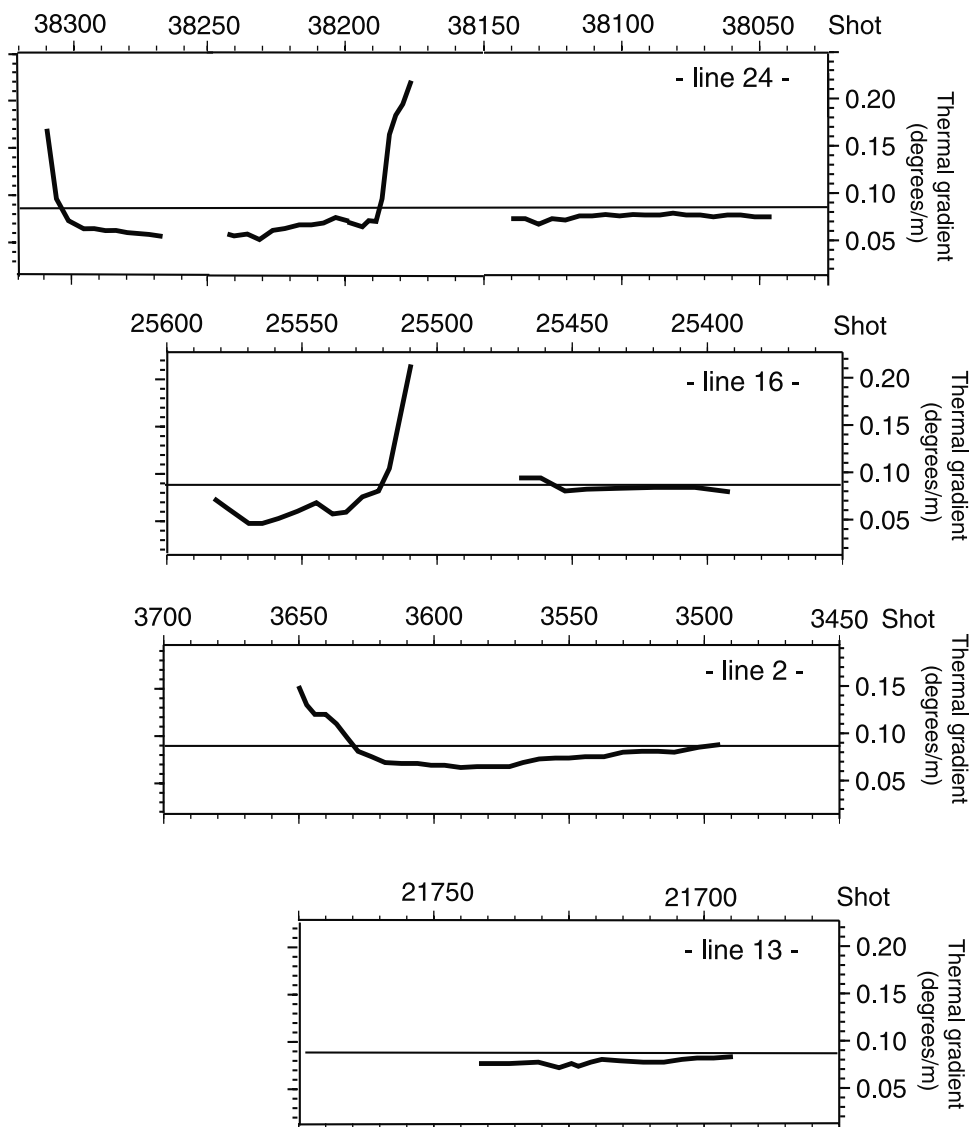
Figure 8. Apparent temperature gradient calculated from observations of BSR depth with the assumptions discussed in section 4. Horizontal gray line marks the measured thermal gradient at ODP site 1022.

these gullies and the increase in the apparent thermal gradient beneath the face of the escarpment, shown by arrows on Figure 4, suggests that these channels are formed by sapping, a geomorphic process whereby groundwater flowing to a sloping surface removes granular material, leading to erosion and eventual undermining of the slope [e.g., *Malin and Edgett*, 2000; *Pederson*, 2001]. This process appears to have led to slumping on lines 24 and 13, removing the sediment and exposing basement on the face of the escarpment on line 13 [*Stakes et al.*, 2002] (Figure 4).

[28] Figure 10 shows calculations of the effect of fluid flow on the apparent temperature gradient near the seafloor. Calculations for three special cases are shown for a simple one-dimensional model of upwelling fluid flow [*Turcotte and Schubert*, 1982, equation 9–113]: $T = T_r - (T_r - T_o)\exp(\rho_f \, c_{pf} v \lambda_m^{-1} y)$, where T_r is temperature of the fluid reservoir, T_o is the surface temperature, ρ_f and c_{pf} are the density and heat capacity of the fluid, v is the velocity of fluid flow, λ_m is an effective thermal conductivity of the rock/fluid system, and y is depth beneath the surface. In case I, flow is assumed to initiate where $T_r - T_o$ is 165°C and the upwelling solution is added to the conductive solution for a temperature gradient of 0.088°C/m. Case II is the same as case I except that the temperature difference is 100°C. Case III is the same as case I except that the conductive temperature gradient is 0°C/m. Calculations are shown for velocities of upward flow of 0.3 and 3 cm/yr because these velocities bracket the range of apparent temperature gradients. An effective thermal conductivity of 1 W m^{-1}°C^{-1} was assumed. Uncertainties in this parameter are inversely proportional to fluid velocity. For example, if $\lambda_m = 3$ W m^{-1}°C^{-1}, which is probably an upper limit on this parameter, then calculations shown correspond to flow rates of 0.1 and 1 cm/yr.

[29] This simple exercise shows that all of the observations of apparent temperature gradient can be explained by
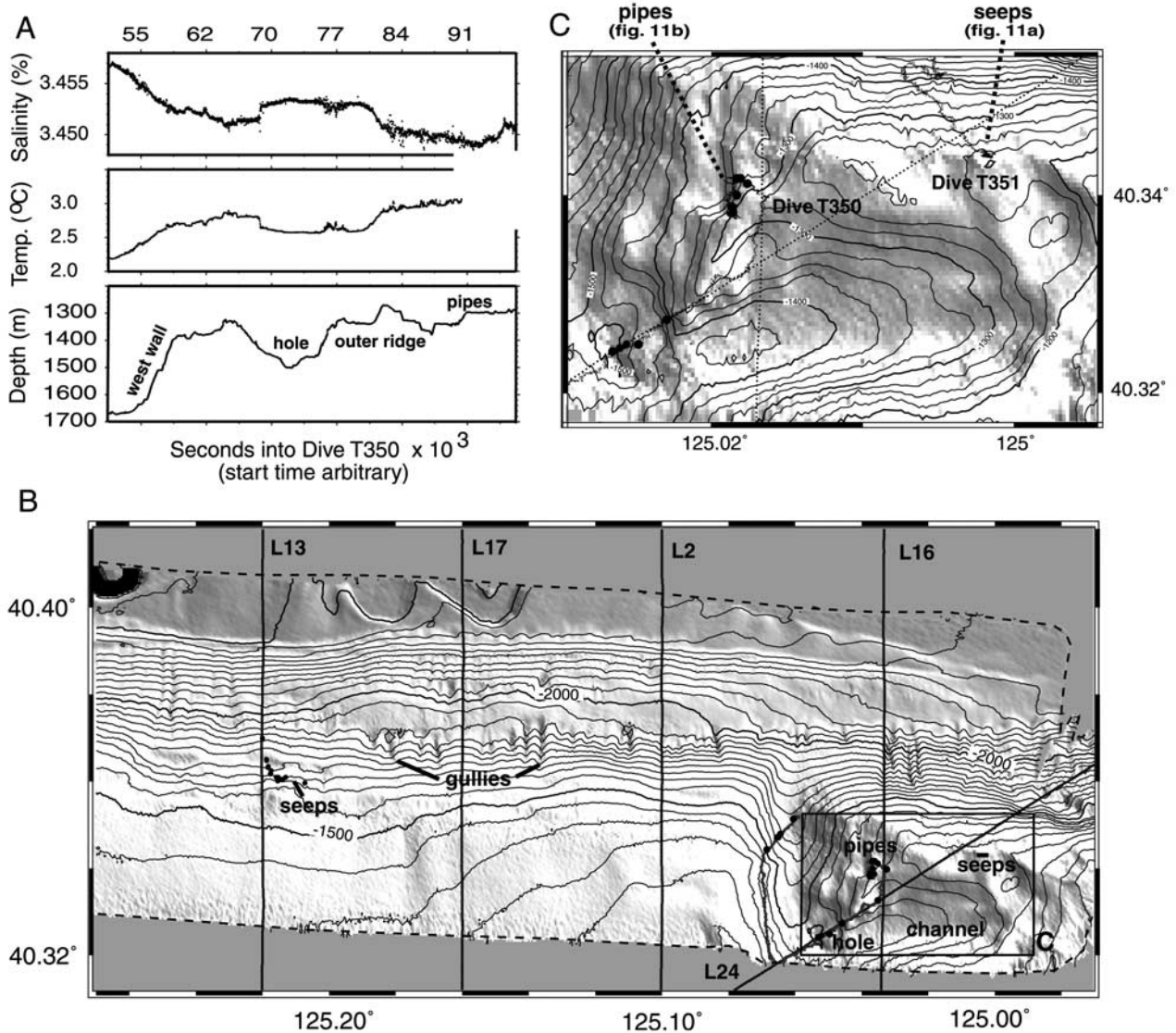
Figure 9. (a) Profiles of water depth, temperature and salinity along the track of ROV Tiburon dive T350 as a function of elapsed time during the dive. The dive track is shown in Figures 9b and 9c. A colder, saltier water mass flows down the axis of the channel, but the seafloor temperature difference is not adequate to explain the observed change in BSR depth for reasons discussed in the text. There is no indication of any temperature or salinity anomalies associated with the hole in the floor of the channel. (b) High-resolution EM300 topographic data showing small headless canyons (gullies) along the face of the Gorda Escarpment and locations of seeps and carbonate pipes found during ROV dives. (c) Detail of the bathymetry of the channel and outer ridge imaged on seismic lines 16 and 24 and explored during dives T350 and T351. Dive track is a gray line; dots show sample locations.

fluid flow velocities <3 cm/yr. It also suggests for flow rates 3 cm/yr, the thickness of the hydrate stability zone will approach 0 and the BSR will disappear, as is sometimes observed beneath fluid expulsion features in accretionary complexes [e.g., *Tréhu et al.*, 1999; *Riedel et al.*, 2001].

[30] *Dugan and Flemings* [2000] calculated that lateral flow rates of ~1 cm/yr could be induced in sediments by topographically and structurally generated pressure gradients on the Atlantic continental margin and speculated that such flow could be responsible for cold seeps and slope

failure there and on passive continental margins world wide. The flow rates we infer from the observed BSR depth are of the same order of magnitude and extend this process to active margins. They are also similar to estimates of diffuse fluid flow rates obtained by various geochemical and geophysical means in clam beds on the Cascadia margin and an order of magnitude smaller than estimates obtained from bacterial mats [*Torres et al.*, 2002].

[31] The small decrease in apparent thermal gradient on lines 2, 16, and 24 as the escarpment is approached from the south may indicate lateral conductive heat
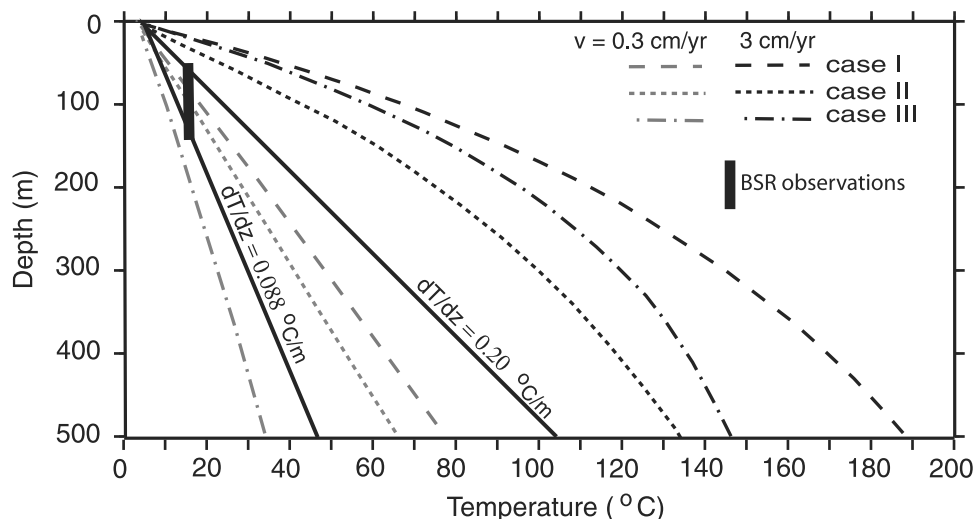
Figure 10. Subsurface temperatures predicted by a simple model of vertical fluid flux for the three cases discussed in the text and for upward (negative) flow velocities of −0.3 and −3.0 cm/yr. Lines showing the thermal gradient measured at ODP Site 1022 and for a thermal gradient of 0.20°C/m are shown for comparison. Bold vertical line shows the range of BSR depths. Because the BSR does not contain any information on the shape of the subsurface temperature profile, it is not possible to separate conductive and convective contributions to the temperature profile.

transport toward the escarpment, which has cooled the edge of the plate. Alternatively, the observed deep BSR may indicate recent unequilibrated uplift and tilting, such that the BSR records the stability boundary at a previous time.

4.2. Discussion of Anomalies Beneath the Channel

[32] The large, local increase in the apparent thermal gradient and gaps in the BSR beneath the 2-km-wide channel near the crest of the escarpment east of 125°6'W suggest upward fluid flow and/or recent removal of sediment from the channel. Seismic data across the channel and outer ridge are quite complicated, suggesting the presence of several large positive and negative velocity contrasts (Figure 11a). An apparent positive-polarity reflection below the BSR may indicate the base of free gas. Possible negative-polarity reflections above the BSR on line 24 suggest the presence of free gas within the hydrate stability zone. A weaker, deeper reflection on line 16 near the predicted depth of the hydrate stability boundary (indicated by a question mark) may be either a relict indicating the position of the BSR prior to an episode of fluid flow or a recent feature indicating reequilibration afterward. No comparable reflection is seen on line 24.

[33] An important question with implications for evaluating the potential of the Gorda Escarpment for tsunamogenic slope failure is whether the channel is a response to deeply rooted faulting or whether it is of shallow origin. A channel on the continental margin of the southeast United States with similar dimensions and morphology was originally interpreted to indicate a series of deeply rooted cracks [*Driscoll et al.*, 2000]; seismic reflection data acquired in 2001, however, indicated that it was underlain by unbroken gas-rich sedimentary horizons, and it is now thought to be the result of a series of gas blowouts (available at http://www.earthinstitute.columbia.edu/news/story5_4.html).

Here, the data suggest the presence of a graben beneath the present axis of the channel that was formed prior to sedimentation (Figure 11b). Overlying strata cannot be traced continuously beneath the outer ridge. Disruptions of strata north of the graben suggest that the graben has been reactivated as a strike-slip fault. We conclude that although the channel may have formed by gas blowouts, the location of the channel is probably controlled by basement tectonic activity. Higher-resolution data are needed to image these structural details more precisely.

5.   Seafloor Seep Indicators

[34] During August 2000 and 2001, we explored the face of Gorda Escarpment using the MBARI remotely operated vehicle (ROV) Tiburon. Four dives, one in 2000 and three in 2001, were located within the region where the BSR is observed. During two dives, which were designed to explore the seafloor where the BSR appears to intersect basement ridge B1 on seismic line 13 (Figures 4 and 9), seep communities comprising vesicomyid clams and tubeworms were discovered on basaltic rocks exposed at the seafloor at 1600 m depth. The geologic setting and faunal assemblages of these seeps are discussed in detail by *Stakes et al.* [2002]. We speculate that this site represents an end-member example of the erosional sapping process described in the previous section. In this scenario, fluids rich in methane flow from beneath the BSR on the south flank of the Gorda Escarpment through fractured and permeable basement rocks of B1 to the seafloor, where sediment that previously draped the slope was undermined and slumped away, exposing basement.

[35] On the basis of experience in the Cascadia subduction zone, where seep sites are often found on local topographic highs overlying areas with strong BSRs, we visited a local high on the outer ridge during dive T351, where we
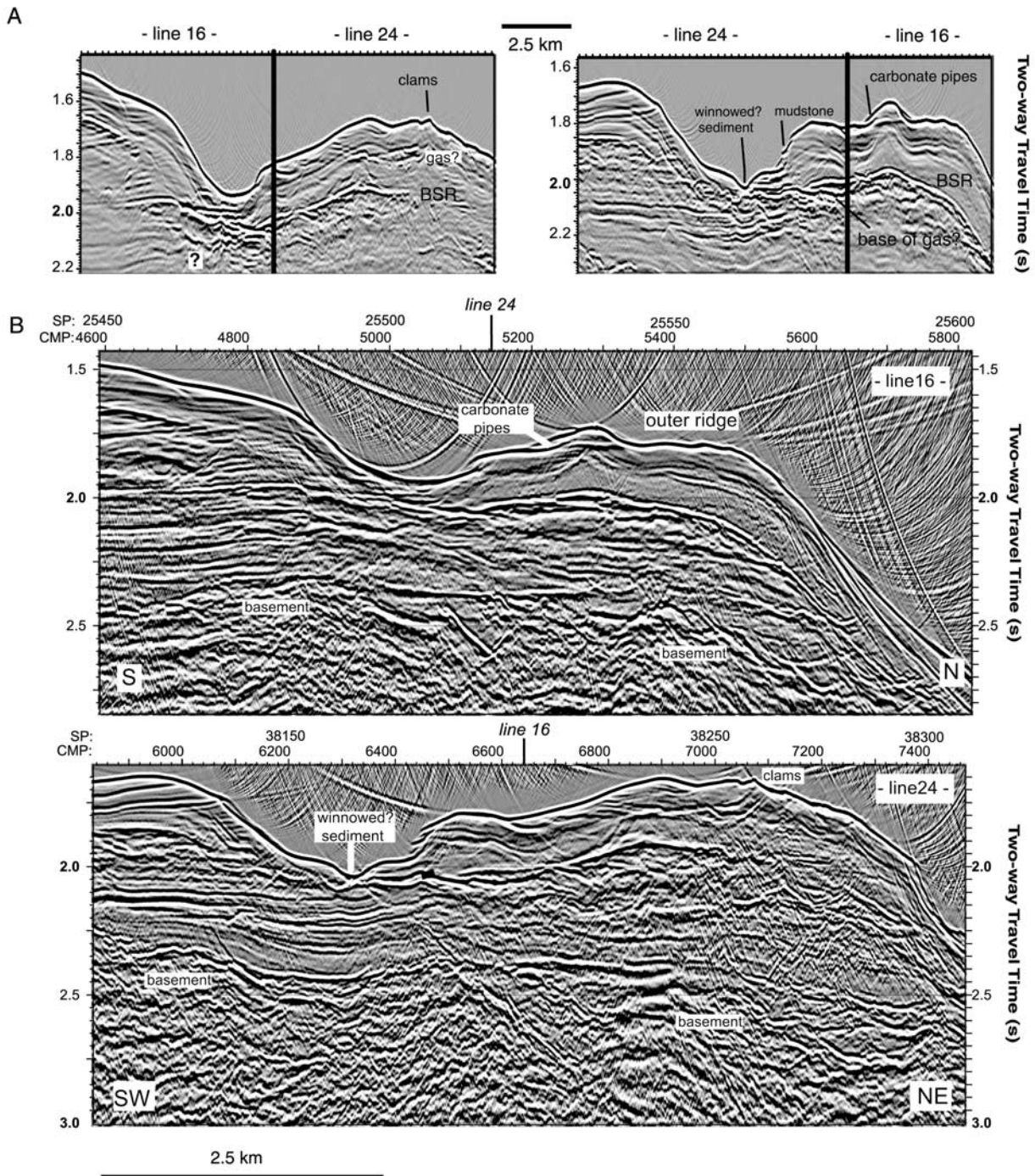
Figure 11. Detail of seismic lines 16 and 24 across the channel near the crest of the escarpment. (a) Data have been f-k (frequency-wave number) migrated with a constant velocity of 1.5 km/s and are shown with relative true amplitudes preserved. (b) Data have been f-k migrated with a constant velocity of 1.7 km/s, which provides the best image of basement. Automatic gain with a window length of 0.5 s has also been applied to emphasize low-amplitude reflections. Locations are shown of seafloor observations discussed in the text. Overmigration of subsurface events on the northern end of the line indicates that velocities here are significantly lower than 1.7 km/s, probably due to the presence of gas.
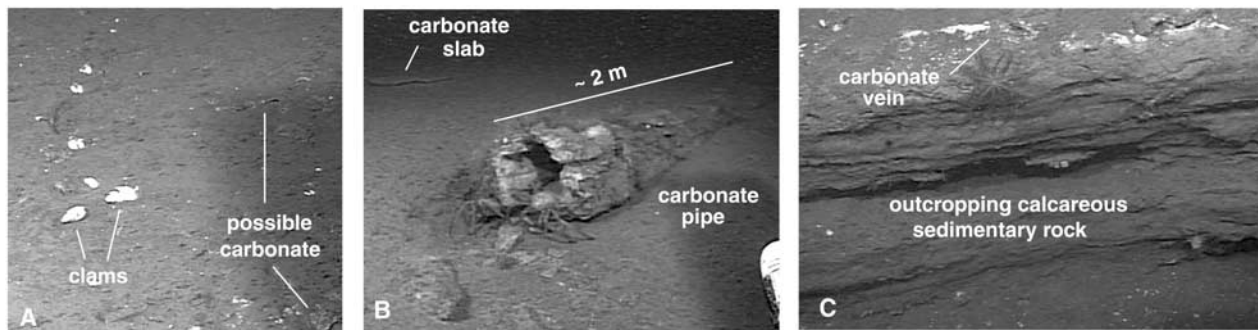
Figure 12. (a) Vesicomyid clams on the seafloor at the crest of the escarpment. In contrast to many seep sites where clams are clustered, here individual clams are sparsely distributed in lines parallel to topography. No bacterial mats, bubbles, or other signs of vigorous fluid flow were observed. Thin carbonate layers beneath a thin sediment cover are seen to the right of the clams. (b) A carbonate pipe, one of several seen near the crest of the escarpment. (c) Carbonate outcrop exposed on the slope beneath the pipes.

observed vesicomyid clams. These seeps are characterized by sparse clams aligned parallel to the axis of the ridge (Figure 12a), suggesting that tensional cracks along the edge of the escarpment are allowing fluids to migrate to the seafloor. They overlie a gap in the BSR on seismic line 24 (Figure 11b). Disappearance of the BSR beneath the seeps is consistent with rapid migration of fluids from beneath the BSR to the seafloor and is perhaps indicative of local tectonic instability and fracturing of carbonate-cemented sediments.

[36] Indications of an earlier episode of venting, in the form of carbonate pipes exposed by seafloor slumping and erosion (Figure 11b), were found farther west on the outer ridge during dive T350 (Figure 9c). The pipes overlie slabs of outcropping carbonate-cemented sedimentary rock containing carbonate veins (Figure 11c). Whether they were originally parallel or perpendicular to bedding is uncertain. Preliminary analyses of oxygen and carbon isotopes in these samples provide additional information on their origin (Figure 13). Eight out of 10 samples from the outer ridge (including all of the pipe samples) have $\delta^{13}C$ values between −32‰ and −36‰ and $\delta^{18}O$ values between 5.2‰ and 6.1‰. These isotopic values are similar to those of carbonates recovered from chemoherms associated with gas hydrates on Hydrate Ridge in the Cascadia subduction zone, falling entirely within group II of *Kulm and Suess* [1990] and close to groups C and D of *Greinert et al.* [2001]. The $\delta^{13}C$ values < −32‰ indicate formation at shallow subseafloor depths through oxidation of methane derived from either biogenic or thermogenic origins [*Greinert et al.*, 2001]. Two samples from this region have high $\delta^{13}C$ values of ∼10 ‰. Similar isotopic compositions are also found in samples from Hydrate Ridge (group A of *Greinert et al.* [2001]), at ODP site 1022 [*Stakes et al.*, 2002], and on the Blake Ridge [*Rodriguez et al.*, 2000]. Such refractory values of $\delta^{13}C$ reflect fluids that are derived from a deeper subsurface zone of methanogenesis remaining after the ^{12}C-enriched methane has been removed [*Greinert et al.*, 2001]. This suggests that lithification of these samples occurred prior to an episode of uplift and erosion that was followed by formation of the pipes. X-ray diffraction analysis of two of these samples indicates that the carbonate phase is dominated by low-Mg calcite, with some ankerite.

[37] Samples from outcrops along the walls of a topographic depression in the floor of the channel (labeled "hole" in Figures 9b and 9c) are dolomites with $\delta^{13}C$ values of 11‰ to 20‰, similar to group I of *Kulm and Suess* [1990], which were from dolomite chimneys recovered from the Oregon continental shelf. Such carbon isotopic compositions could either be derived from normal marine particulate organic carbon ($\delta^{13}C \approx -20‰$) and shallow aerobic processes or from thermogenic methane and/or reduced carbon dioxide derived from a deep source transported along a fault.

[38] We were surprised to find seep no communities or signs of fluid flow in bottom water temperature and salinity recorded by the ROV in the floor of the channel. The hole, however, contains a coarse grained sand (>350 μm) composed primarily of glauconitic pellets and benthic foraminifera (A. Mix, personal communication, 2001), in contrast to sediment samples from basins on the walls of the channel, which are fine-grained and contain only planktonic microfossils. The abundance of benthic foraminifera suggests high benthic productivity, and one possible explanation for the coarse grain size is winnowing of sediment grains by fluid flow. Whether these characteristics are related to cold seeps is unclear.

6. Evidence for Uplift Near the Triple Junction

[39] As discussed above, there is evidence for gas throughout the sedimentary basin south of the Gorda Escarpment. So why is the BSR observed only near the escarpment? One possible explanation is that hydrate is present within a broader region around the boundary of the marginal basin and that the BSR is a result of destabilization of the base of the gas hydrate stability field because of geographically limited current uplift that is occurring in response to triple junction tectonics. A similar mechanism has been proposed to explain why sediments recovered from tectonically uplifted regions with a strong BSR sometimes indicate only a small amount of dispersed hydrate in the sediments above the BSR, whereas sediments containing
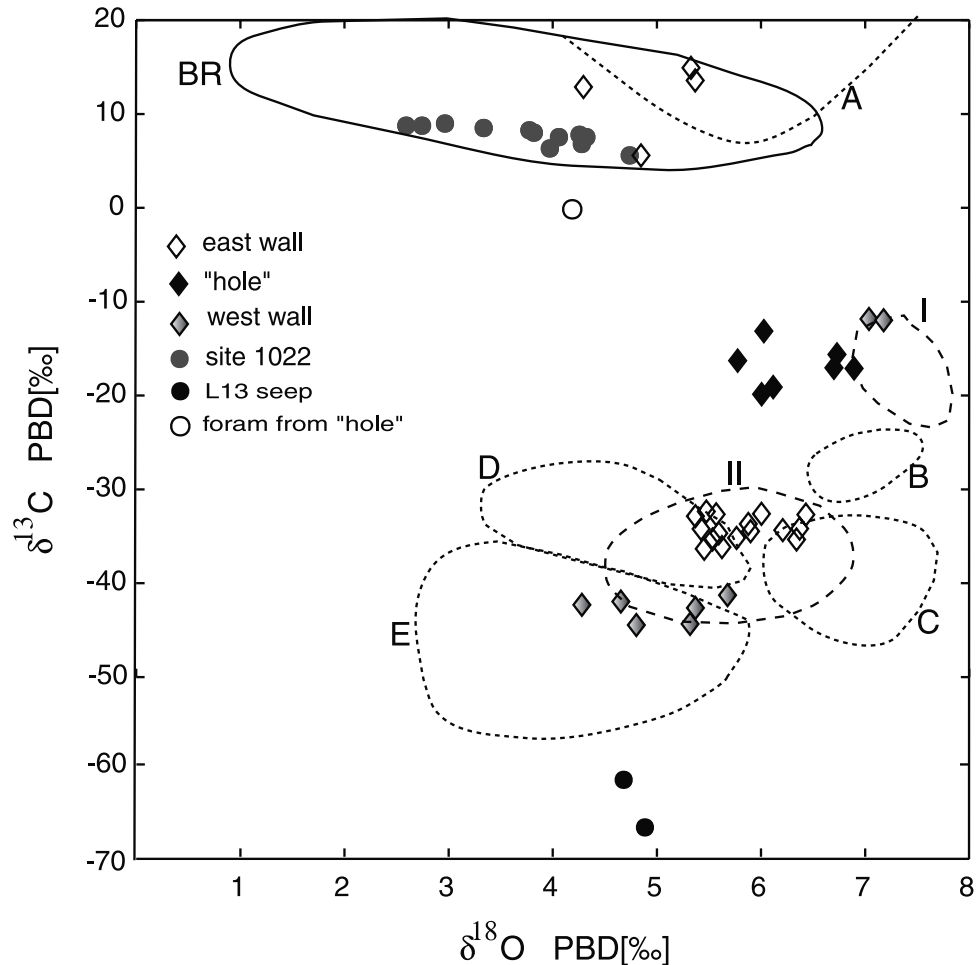
Figure 13. Stable isotope compositions of carbonates from dive T350. Results from two to four subsamples of each sample are plotted. Uncertainties for each point are 0.02 or smaller. Subsamples from the same sample gave consistent results in all cases. The result from a benthic foraminifera from the floor of the hole is also shown and is consistent with seawater. Results for ODP Site 1022 dolomites and for high-Mg calcites from the line 13 seep site are from *Stakes et al.* [2002]. Long dashed outlines are fields I and II defined from samples from the Oregon continental shelf and outer accretionary complex, respectively [*Kulm and Suess*, 1999]; short dashed outlines are fields A to E defined by many samples from Hydrate Ridge in the Oregon accretionary complex [*Greinert et al.*, 2001]; the solid (BR) outlines is the field defined by dolomites from within the hydrate stability zone at ODP Site 195 on the Blake Ridge [*Rodriguez et al.*, 2000].

larger amounts of hydrate have been recovered from subsiding regions where no BSR is detected [*Pecher et al.*, 1996, 2001]. Tectonic uplift results in a decrease in pressure at the base of the hydrate stability zone, moving this boundary to shallower stratigraphic depth and leading to dissociation of hydrates and generation of free gas at the stratigraphic depth of the old stability boundary.

[40] Seismic sections crossing the Gorda Escarpment image a series of basement ridges (labeled B1 and B2 in Figure 2c). These ridges and the overlying sediments document a long history of uplift and subsidence along the Gorda Escarpment (Figure 14). Uplift was greatest along the central part of the escarpment from 125°20' to 125°36', where no negative-polarity BSR is observed. Here the basement ridge is exposed at the seafloor, erosion has exposed sediments as old as late Miocene, and late Pliocene

subsidence followed uplift. Earthquake source mechanisms indicate that present-day motion along this portion of the Mendocino transform fault is purely strike slip (Figure 15). We therefore conclude that B1 is a relict of early to mid-Pliocene uplift. Any free gas that might have been released by hydrate dissociation during this earlier episode of uplift has apparently been reincorporated into hydrate, dissolved in the pore water, or removed by fluid flow.

[41] In contrast, earthquake mechanisms near the triple junction are highly variable, and several mechanisms contain a large component of dip-slip motion. Onshore, very rapid uplift rates have been documented in the King Range, a sliver of North America that is apparently in the process of being captured by the Pacific plate as the primary locus of Pacific/North America plate motion is being transferred inland from the San Andreas fault [*McLaughlin et al.*,
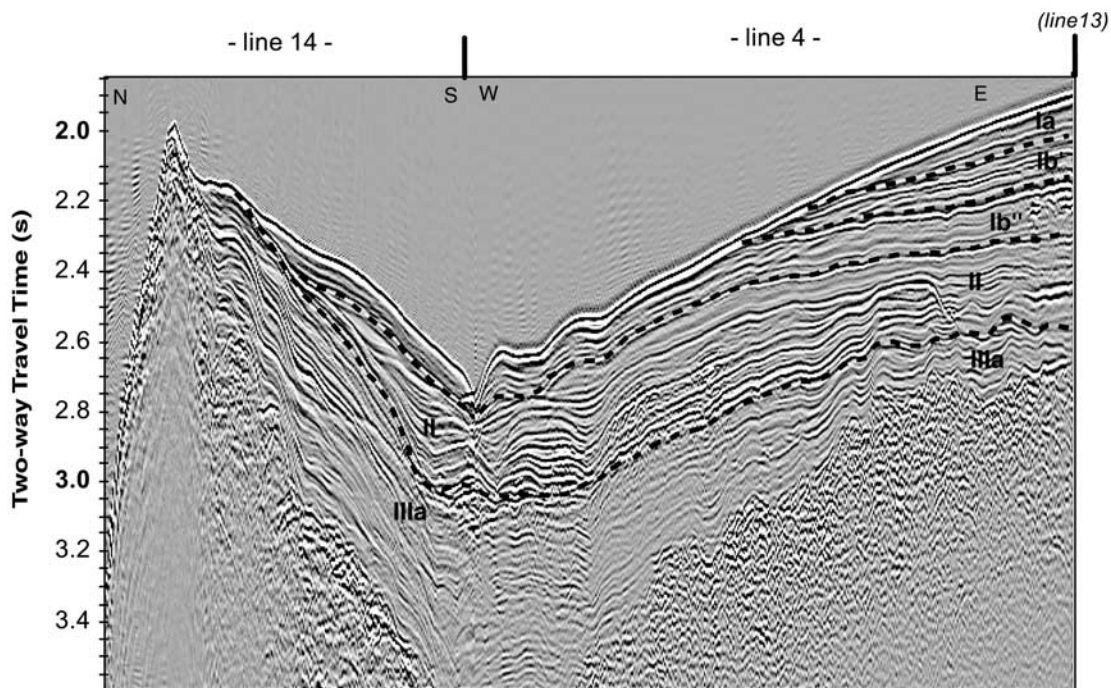
Figure 14. A seismic line across the central part of the Gorda Escarpment and the tie along line 4 to line 13, which is shown in Figure 4. Stratigraphic correlations indicate that uplift along this western part of the escarpment has been followed by subsidence. Details of this earlier uplift and subsidence history will be discussed elsewhere.

1997]. On the basis of topography and seismicity, several oblique faults can be inferred to accommodate deformation in the transition zone from the San Andreas fault to the Mendocino fault (Figure 15). These faults extend into the region where the BSR is observed. We suggest that this region is being uplifted as part of the present triple junction regime and that basement ridges labeled B2 in Figure 2c are currently active. This interpretation is consistent with the observation that the BSR disappears as basement deepens to the south.

[42] An alternative explanation for the limited extent of the BSR is that fluid flow is almost exclusively along stratigraphic interfaces and that only stratigraphic units Ib″ and II have high enough methane concentrations to support hydrate and free gas formation. With this explanation, the BSR is not observed to the south because younger sediments with lower methane content are in the hydrate stability field. This explanation, however, does not explain the disappearance of the BSR to the west, where the same stratigraphic horizons intersect the hydrate stability zone.

[43] We note that uplift along the Mendocino transform is not surprising given the large compressive component across the transform predicted by global solutions for current Pacific and Gorda plate motions [*DeMets et al.*, 1994]. What is surprising is the apparent absence of contemporary uplift along most of the Mendocino transform fault. At present, most of the Pacific/Gorda component of compression is taken up by deformation within the Gorda plate. In the past, it appears to have been taken up by crustal thickening and uplift in the transform zone and by shortening within the Pacific plate [*Leitner et al.*, 1998]. The

mechanism for accommodating compression probably depends on the age of the plates on either side of the transform, which changes with time. At present the Pacific plate is generally older and stronger than the Gorda plate. The age contrast decreases toward the east [*Leitner et al.*, 1998], increasing the likelihood of contemporary deformation and uplift within the Pacific plate.

7. Summary

[44] We have documented the presence of seismic indicators of free gas, and indirectly of gas hydrate, on the California transform margin near the eastern end of the Mendocino transform fault. Although free gas occurs throughout the basin south of the transform, as indicated by classic gas indicators such as bright spots and gas curtains, a bottom simulating reflection (BSR) indicative of the presence of hydrate-bearing sediments overlying sediments containing free gas is observed only within 6 km of the escarpment near the Mendocino triple junction. The amplitude of the BSR is comparable to that determined for strong BSRs in the Cascadia accretionary complex and Blake Ridge.

[45] Interval velocity analysis indicates velocities as low as 1.38 km/s in layers up to 200–300 m thick beneath the BSR, indicating that free gas is present in the pore space. Interval velocities of the sediments within the hydrate stability zone show only a small (at most 0.05 km/s) and poorly constrained contrast in velocity between locations where the BSR is detected and those where it is not observed. This implies little change in the hydrate concen-
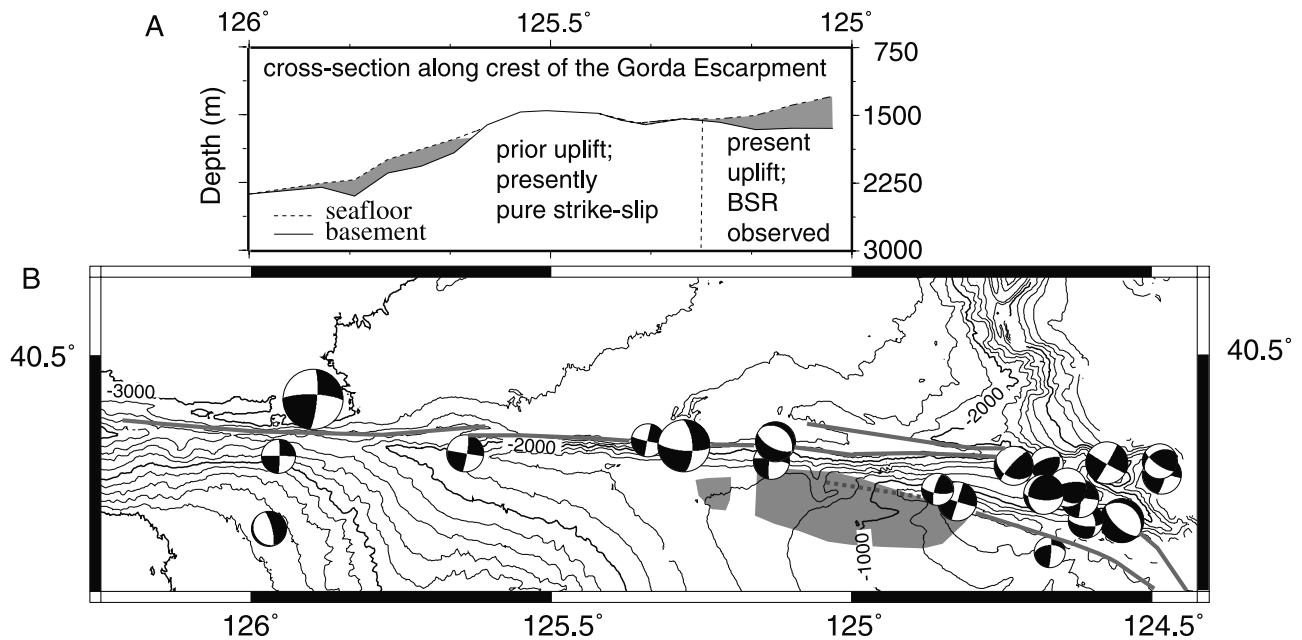
Figure 15. (a) Cross section showing the seafloor and basement along the crest of the Gorda Escarpment. (b) Fault mechanisms of all events from 1990 to 2000 (from the Berkeley Northern California network on-line catalog (available at http://www.seismo.berkeley.edu/~dreger/mtmaps.html). Mechanism symbols are centered on the epicenter, with radius proportional to magnitude. Shaded area shows where BSR is observed. Grey lines show strands of the San Andreas and Mendocino transform faults inferred from topography and seismicity.

tration between where the BSR is observed and where it is absent, indicating either that the concentration is low or that hydrate is present south of where the BSR is observed. We tentatively interpret a regional pattern of discontinuous reflection segments that are parallel to the seafloor and oblique to strata to suggest the latter.

[46] Fluid flow toward the escarpment is interpreted from anomalies in the depth of the BSR, from seafloor gullies on the face of the escarpment that may be caused by escaping groundwater, and from seafloor observations of cold seep communities. A simple model of the thermal perturbation expected from vertical fluid flow suggests flow rates of <3 cm/yr. These estimates are consistent with estimates obtained by a variety of approaches at other continental margin sites. The model also suggests that larger flow rates should result in extreme shallowing and disappearance of the BSR, as is sometimes observed beneath fluid expulsion features in hydrate-bearing regions.

[47] Carbon and oxygen isotopic composition of carbonates recovered from the seafloor are similar to those of carbonates from other hydrate-bearing regions and can be grouped into several distinct categories that provide constraints on their origin. Carbonate pipes found near the crest of the escarpment have a carbon isotopic signature very similar to that of chemoherms from Hydrate Ridge on the Oregon accretionary margin and suggest a primarily methane source. A few samples with high values of $\delta^{13}C$ indicate formation from refractory CO_2 within a deeper zone of methanogenesis.

[48] The primary significance of this study is that it provides the first detailed documentation of a major hydrate/free gas system along a transform margin. More-

over, it suggests that the mechanism for focusing methane in concentrations adequate to form hydrate is somewhat different from the mechanisms proposed for accretionary complexes like Cascadia, where sediment subduction may help to feed the system from below, and the Blake Ridge, where very fast deposition of organic rich sediment may cause the base of the gas hydrate stability zone to migrate upward, releasing free gas that then migrates back into the stability zone. Here, the seismic data suggest that basin-wide flow, primarily along stratigraphic horizons, transports methane to the tectonically uplifted edge of the basin. In this model, hydrate that has formed in the tectonically uplifted sediments is destabilized by continuing uplift, leading to local formation of the BSR.

[49] In addition, there is tentative evidence in a channel along the crest of the escarpment beneath which the BSR is anomalously shallow that basement tectonic activity may result in occasional explosive gas release. Additional data are needed to determine whether this feature is still active and whether it is gravitationally unstable, thus posing a tsunami hazard to coastal communities in northern California.

References

Aiello, I. W., R. E. Garrison, J. C. Moore, M. Kastner, and D. S. Stakes, Anatomy and origin of carbonate structures in a Miocene cold seep field, *Geology*, *29*, 1111–1114, 2001.

Bangs, N. L. B., D. S. Sawyer, and X. Golovchenko, Free gas at the base of the gas hydrate zone in the vicinity of the Chile triple junction, *Geology*, *21*, 905–908, 1993.

Brooks, J. M., M. E. Field, and M. C. Kennicutt, Observations of gas hydrates in marine sediments offshore northern California, *Mar. Geol.*, *96*, 103–109, 1991.

Carcione, J. M., and U. Tinivella, Bottom simulating reflectors: Seismic velocities and AVO effect, *Geophysics*, *65*, 54–67, 2000.

Carson, B., G. K. Westbrook, R. J. Musgrave, and E. Suess, *Proceedings of the Ocean Drilling Program, Scientific Results*, part 1, vol. 146, 467 pp., Ocean Drill. Program, College Station, Tex., 1995.

Claerbout, J. F., *Fundamentals of Geophysical Data Processing*, 274 pp., Blackwell Sci., Malden, Mass., 1976.

Clennell, M. B., M. Hovland, J. S. Booth, P. Henry, and W. J. Winters, Formation of natural gas hydrates in marine sediments: 1. Conceptual model of gas hydrate growth conditioned by host sediment properties, *J. Geophys. Res.*, *104*, 22,985–23,004, 1999.

DeMets, C., R. G. Gordon, D. F. Argus, and S. Stein, Effect of recent revisions to the geomagnetic reversal time scale on estimate of current plate motions, *Geophys. Res. Lett.*, *21*, 2191–2194, 1994.

Dickens, G. R., Modeling the global carbon cycle with a gas hydrate capacitor: Significance for the latest Paleocene thermal maximum, in *Natural Gas Hydrates: Occurrence, Distribution and Detection*, *Geophys. Monogr. Ser.*, vol. 124, edited by C. K. Paull and W. P. Dillon, pp. 19–40, AGU, Washington, D. C., 2001.

Driscoll, N. W., J. K. Weissel, and J. A. Goff, Potential for large-scale submarine slope failure and tsunami generation along the U. S. mid-Atlantic coast, *Geology*, *28*, 407–411, 2000.

Dugan, B., and P. B. Flemings, Overpressure and fluid flow in the New Jersey continental slope: Implications for slope failure and cold seeps, *Science*, *289*, 288–291, 2000.

Eichhubl, P., and J. R. Boles, Focused fluid flow along faults in the Monterey Formation, coastal California, *Geol. Soc. Am. Bull.*, *112*, 1667–1679, 2000.

Fink, C. R., Methane hydrate distribution offshore Vancouver Island from detailed single channel seismic, M.S. thesis, 110 pp., Sch. of Earth and Ocean Sci., Univ. of Victoria, Toronto, Ont., 1995.

Fink, C. R., and G. D. Spence, Hydrate distribution off Vancouver Island from multifrequency single channel seismic reflection data, *J. Geophys. Res.*, *104*, 2909–2922, 1999.

Gorman, A. R., W. S. Holbrook, M. J. Hornbach, K. L. Hackwith, D. Lizzeralde, and I. Pecher, Migration of methane gas through the hydrate stability zone in a low-flux province, *Geology*, *30*, 327–330, 2002.

Greinert, J., G. Bohrmann, and E. Suess, Gas hydrate-associated carbonates and methane-venting at Hydrate Ridge: Classification, distribution and origin of authigenic lithologies, in *Natural Gas Hydrates: Occurrence, Distribution and Detection*, *Geophys. Monogr. Ser.*, vol. 124, edited by C. K. Paull and W. P. Dillon, pp. 199–114, AGU, Washington, D. C., 2001.

Han, D., and M. Batzle, Fizz water and low gas-saturated resevoirs, *Leading Edge*, *21*, 395–398, 2002.

Holbrook, W. S., Seismic studies of the Blake Ridge: Implications for hydrate distribution, methane expulsion, and free gas dynamics, in *Natural Gas Hydrates: Occurrence, Distribution and Detection*, *Geophys. Monogr. Ser.*, vol. 124, edited by C. K. Paull and W. P. Dillon, pp. 235–256, AGU, Washington, D. C., 2001.

Holbrook, W. S., H. Hoskins, W. T. Wood, R. A. Stephen, D. Lizarralde, and Leg 164 Science Party, Methane hydrate and free gas on the Blake Ridge from vertical seismic profiling, *Science*, *273*, 1840–1843, 1996.

Hovland, M., and P. V. Curzi, Gas seepage and assumed mud diapirism in the Italian central Adriatic Sea, *Mar. Pet. Geol.*, *6*, 161–169, 1989.

Hovland, M., A. Judd, and P. Soderberg, Gas accumulation in, and migration through low-permeability, fine-grained sediments, in, paper presented at AAPG Hedberg Research Conference on Near-Surface Expression of Hydrocarbon Migration, Am. Assoc. of Pet. Geol., Vancouver, B. C., 24–28 April 1994.

Hyndman, R. D., G. F. Moore, and K. Moran, Velocity, porosity and pore-fluid loss from the Nankai subduction zone accretionary prism, *Proc. Ocean Drill. Program Sci. Results*, *131*, 211–220, 1993.

Katzman, R., W. S. Holbrook, and C. K. Paull, Combined vertical-incidence and wide-angle seismic study of a gas hydrate zone, Blake Ridge, *J. Geophys. Res.*, *97*, 17,975–17,995, 1994.

Korenaga, J., W. S. Holbrook, S. C. Singh, and T. A. Minshull, Natural gas hydrates on the SE US margin: Constraints from full waveform inversions of wide-angle seismic data, *J. Geophys. Res.*, *102*, 15,345–15,365, 1997.

Kulm, L. D., and E. Suess, Relationship between carbonate deposits and fluid venting: Oregon accretionary prism, *J. Geophys. Res.*, *95*, 8899–8915, 1990.

Kvenvolden, K. A., and M. Kastner, Gas hydrate of the Peruvian outer continental margin, *Proc. Ocean Drill. Program Sci. Results*, *112*, 517–526, 1990.

Kvenvolden, K. A., and T. D. Lorenson, The global occurrence of natural gas hydrates, in *Natural Gas Hydrates: Occurrence, Distribution and Detection*, *Geophys. Monogr. Ser.*, vol. 124, edited by C. K. Paull and W. P. Dillon, pp. 3–18, AGU, Washington, D. C., 2001.

Leg 167 Shipboard Scientific Party, Leg 167 introduction, Sites 1010–1022, California margin, *Proc. Ocean Drill. Program Initial Rep.*, part 1, *167*, 5–14, 1997a.

Leg 167 Shipboard Scientific Party, Site 1022, Sites 1010–1022, California margin, *Proc. Ocean Drill. Program Initial Rep.*, part 1, *167*, 5–14, 1997b.

Leitner, B., A. M. Tréhu, and N. Godfrey, Crustal structure of the northwestern Vizcaino Block and Gorda Escarpment offshore northern California: Implications for the influence of plate age on internal deformation, *J. Geophys. Res.*, *103*, 23,795–23,812, 1998.

Lyle, M., I. Koizumi, M. L. Delaney, and J. A. Barron, Sedimentary record of the California Current system, middle Miocene to Holocene: A synthesis of Leg 167 results, *Proc. Ocean Drill. Program Sci. Results*, *167*, 341–378, 2000.

MacKay, M. E., R. D. Jarrad, G. K. Westbrook, R. D. Hyndman, and Shipboard Scientific Party, ODP Leg 146, origin of BSRs: Geophysical evidence from the Cascadia accretionary prism, *Geology*, *22*, 459–462, 1994.

Maekawa, T., S. Itoh, S. Sakata, S. Igari, and N. Imai, Pressure and temperature conditions for methane hydrate dissociation in sodium chloride solutions, *Geochem. J.*, *29*, 325–329, 1995.

Malin, M. C., and K. S. Edgett, Evidence for recent groundwater seepage and surface runoff on Mars, *Science*, *288*, 2330–2335, 2000.

McLaughlin, R. J., W. V. Sliter, N. O. Frederikson, and W. P. Harbert, Plate motions recorded in tectonostratigraphic terranes of the Franciscan complex and evolution of the Mendocino triple junction, northwestern California, *U.S. Geol. Surv.*, 60, 1997.

Ostrander, W. J., Plane-wave reflection coefficients for gas sands at non-normal angles of incidence, *Geophysics*, *49*, 1637–1648, 1984.

Paull, C. K., and W. Ussler III, History and significance of gas sampling during the DSDP and ODP, in *Natural Gas Hydrates: Occurrence, Distribution and Detection*, *Geophys. Monogr. Ser.*, vol. 124, edited by C. K. Paull and W. P. Dillon, pp. 53–66, AGU, Washington, D. C., 2001.

Paull, C. K., et al., *Proceedings of the Ocean Drilling Program, Initial Reports*, vol. 164, 623 pp., Ocean Drill. Program, College Station, Tex., 1996.

Pecher, I. A., T. A. Minshull, S. C. Singh, and R. von Huene, Velocity structure of a bottom simulating reflector offshore Peru: Results from full waveform inversion, *Earth Planet. Sci. Lett.*, *139*, 459–469, 1996.

Pecher, I. A., N. Kukowski, C. R. Ranero, and R. vonHuene, Gas hydrates along the Peru and Middle America trench system, in *Natural Gas Hydrates: Occurrence, Distribution and Detection*, *Geophys. Monogr. Ser.*, vol. 124, edited by C. K. Paull and W. P. Dillon, pp. 258–272, AGU, Washington, D. C., 2001.

Pederson, D. T., Stream piracy revisited: A groundwater-sapping solution, *GSA Today*, *11*, 4–10, 2001.

Rempel, A., and B. Buffett, Formation and accumulation of gas hydrate in porous media, *J. Geophys. Res.*, *102*, 10,151–10,164, 1997.

Revelle, R. R., Methane hydrates in continental slope sediments and increasing atmospheric carbon dioxide, in *Changing Climates*, pp. 252–261, Natl. Acad. Press, Washington, D. C., 1983.

Riedel, M., G. D. Spence, R. Chapman, and R. D. Hyndman, Deep-sea gas hydrates on the northern Cascadia margin, *Leading Edge*, *20*, 87–109, 2001.

Rodriguez, N. M., C. K. Paull, and W. S. Borowski, Carbonate diagenetic zonations within gas hydrate-bearing sedimentary sections on the Blake Ridge, off southeast North America, *Proc. Ocean Drill. Program Sci. Results*, *164*, 301–312, 2000.

Ruppel, C., Anomalously cold temperatures observed at the base of the gas hydrate stability zone on the US passive margin, *Geology*, *25*, 699–702, 1997.

Scholl, D. W., and P. E. Hart, Velocity and amplitude structures on seismic-reflection profiles-possible massive gas-hydrate deposits and underlying gas accumulations in the Bering Sea Basin, in *The Future of Energy Gases*, edited by D. G. Howell, *U.S. Geol. Surv. Prof. Pap.*, *1570*, 331–351, 1993.

Shipley, T. H., M. H. Houston, R. T. Buffler, F. J. Shaub, K. J. McMillen, J. W. Ladd, and J. L. Worzel, Seismic evidence for widespread possible gas hydrate horizons on continental slopes and rises, *AAPG Bull.*, *63*, 2204–2213, 1979.

Singh, S. C., T. A. Minshull, and G. D. Spence, Velocity structure of a gas hydrate reflector, *Science*, *260*, 204–207, 1993.

Stakes, D. S., A. M. Tréhu, K. A. Salamy, S. K. Goffredi, T. H. Naehr, and R. A. Duncan, Mass wasting, methane venting, and biological communities on the Mendocino transform fault, *Geology*, *30*, 407–410, 2002.

Suess, E., et al., Seafloor methane hydrates at Hydrate Ridge, Cascadia margin, in *Natural Gas Hydrates: Occurrence, Distribution and Detection*, *Geophys. Monogr. Ser.*, vol. 124, edited by C. K. Paull and W. P. Dillon, pp. 87–98, AGU, Washington, D. C., 2001.

Torres, M., Fluid and chemical fluxes in and out of sediments hosting methane hydrate deposits on Hydrate Ridge, OR: 1, Hydrological provinces, *Earth Planet. Sci. Lett.*, *201*, 525–540, 2002.

Tréhu, A. M., G. Lin, E. Maxwell, and C. Goldfinger, A seismic reflection profile across the Cascadia subduction zone offshore central Oregon: New constraints on the deep crustal structure and on the distribution of methane in the accretionary prism, *J. Geophys. Res*, *100*, 15,101–15,116, 1995.

Tréhu, A. M., M. Torres, G. Moore, E. Suess, and G. Bohrmann, Dissociation of gas hydrates in response to slumping and folding on the Oregon continental margin, *Geology*, *27*, 939–942, 1999.

Turcotte, D., and G. Schubert, *Geodynamics: Applications of Continuum Physics to Geological Problems*, 450 pp., John Wiley, New York, 1982.

Wessel, P., and W. H. F. Smith, New version of the Generic Mapping Tools released, *Eos Trans. AGU*, *76*, 329, 1995.

Yamano, M., S. Uyeda, Y. Aoki, and T. H. Shipley, Estimates of heat flow derived from gas hydrates, *Geology*, *10*, 339–343, 1982.

Yuan, T., R. D. Hyndman, G. D. Spence, and B. Desmons, Velocity structure of a bottom-simulating reflector and deep sea gas hydrate concentrations on the Cascadia continental slope, *J. Geophys. Res.*, *101*, 13,655–13,671, 1996.

Yuan, T., G. D. Spence, R. D. Hyndman, T. A. Minshull, and S. C. Singh, Seismic velocity studies of a gas hydrate bottom-simulating reflector on the northern Cascadia continental margin: Amplitude modeling and full waveform inversion, *J. Geophys. Res.*, *104*, 1179–1191, 1999.

Xu, W., and C. Ruppel, Predicting the occurrence, distribution, and evolution of methane gas hydrate in porous marine sediments, *J. Geophys. Res.*, *104*, 5081–5096, 1999.

Zatsepina, O. Y., and B. A. Buffett, Phase equilibrium of gas hydrate: Implications for the formation of hydrate in the deep sea floor, *Geophys. Res. Lett.*, *24*, 1567–1570, 1997.

Zwart, G., J. C. Moore, and G. R. Cochrane, Variations in temperature gradients identify active faults in the Oregon accretionary prism, *Earth Planet. Sci. Lett.*, *139*, 485–495, 1996.

———————————

C. D. Bartlett, AMEC, 7477 SW Tech Center Drive, Portland, OR 97223, USA.

J. Chevallier, R. A. Duncan, S. M. Potter, and A. M. Tréhu, College of Oceanic and Atmospheric Sciences, Oregon State University, Ocean Admin. Bldg. 104, Corvallis, OR 97331-5503, USA. (trehu@coas.oregonstate.edu)

S. K. Goffredi, K. A. Salamy, and D. S. Stakes, Monterey Bay Aquarium Research Institute, 7700 Sandholt Road, Moss Landing, CA 95039-9644, USA.